Geomorphology 273 (2016) 150–167

Contents lists available at ScienceDirect

Geomorphology

journal homepage: www.elsevier.com/locate/geomorph

Integrating expert opinion with modelling for quantitative multi-hazard risk assessment in the Eastern Italian Alps

Lixia Chen [a,b,*], Cees J. van Westen [a], Haydar Hussin [a], Roxana L. Ciurean [c], Thea Turkington [a], Diana Chavarro-Rincon [a], Dhruba P. Shrestha [a]

[a] Faculty of Geo-Information Science and Earth Observation (ITC), University of Twente, Enschede, The Netherlands
[b] Institute of Geophysics and Geomatics, China University of Geosciences, Wuhan, China
[c] Department of Geography and Regional Research, University of Vienna, Vienna, Austria

ARTICLE INFO

Article history:
Received 31 August 2015
Received in revised form 8 June 2016
Accepted 30 July 2016
Available online 2 August 2016

Keywords:
Multi-hazard
Hydro-meteorological hazards
Quantitative risk assessment
Vulnerability
Uncertainty
GIS
Italy

ABSTRACT

Extreme rainfall events are the main triggering causes for hydro-meteorological hazards in mountainous areas, where development is often constrained by the limited space suitable for construction. In these areas, hazard and risk assessments are fundamental for risk mitigation, especially for preventive planning, risk communication and emergency preparedness. Multi-hazard risk assessment in mountainous areas at local and regional scales remain a major challenge because of lack of data related to past events and causal factors, and the interactions between different types of hazards. The lack of data leads to a high level of uncertainty in the application of quantitative methods for hazard and risk assessment. Therefore, a systematic approach is required to combine these quantitative methods with expert-based assumptions and decisions. In this study, a quantitative multi-hazard risk assessment was carried out in the Fella River valley, prone to debris flows and flood in the north-eastern Italian Alps. The main steps include data collection and development of inventory maps, definition of hazard scenarios, hazard assessment in terms of temporal and spatial probability calculation and intensity modelling, elements-at-risk mapping, estimation of asset values and the number of people, physical vulnerability assessment, the generation of risk curves and annual risk calculation. To compare the risk for each type of hazard, risk curves were generated for debris flows, river floods and flash floods. Uncertainties were expressed as minimum, average and maximum values of temporal and spatial probability, replacement costs of assets, population numbers, and physical vulnerability. These result in minimum, average and maximum risk curves. To validate this approach, a back analysis was conducted using the extreme hydro-meteorological event that occurred in August 2003 in the Fella River valley. The results show a good performance when compared to the historical damage reports.

1. Introduction

Hydro-meteorological hazards are processes or phenomena of atmospheric, hydrological or oceanographic nature that may cause loss of life, injury or other health impacts, property damage, loss of livelihoods and services, social and economic disruption or environmental damage (UNISDR, 2009). Shallow or deep-seated landslides, debris flows, rock falls, flash floods and river floods can be triggered simultaneously or consecutively in mountainous areas by extreme hydro-meteorological conditions.

Since more than one hazard types can occur in mountainous areas during the same hydro-meteorological event, it is important to assess the risk in a multi-hazard framework. Compared to single processes, standard approaches and methodological frameworks for multi-hazard risk assessment are less common in the literature. Kappes et al. (2012) indicated that this is due to the different characteristics of hazard types, which also require different methods for analysis. Multi-hazard risk assessment has received a lot of attention in research in the past decades, focusing on the analysis at different scales. For small scales, the World Bank approach (Dilley et al., 2005) or the EU ESPON project (Schmidt-Tomé et al., 2006) could be mentioned. Several EU research projects dealt with the problem of multi-hazard risk assessment at medium scales, such as the TIGRA (Del Monaco et al., 1999), ARMONIA (Del Monaco et al., 2007), MATRIX (Marzocchi et al., 2012; Nadim et al., 2013) and CLUVA (Garcia-Aristizabal et al., 2015). Initiatives for multi-hazard risk assessment at medium to large scales include the EU funded NASRAS (Marzocchi et al., 2009), RISK-NAT (Douglas, 2007) and MEDIGRID (Bovolo et al., 2009) projects; the German DFNK project on a comparative study of multi-hazard risk in Cologne (Grunthal et al., 2006); the Australian Cities project (Granger et al.,

* Corresponding author at: Institute of Geophysics and Geomatics, China University of Geosciences, Wuhan, China.
E-mail address: ch_l_x@163.com (L. Chen).

http://dx.doi.org/10.1016/j.geomorph.2016.07.041
0169-555X/

1999) and several other initiatives (e.g. Van Westen et al., 2002; Carpignano et al., 2009; Lari et al., 2009).

A number of software tools have been developed for multi-hazard risk assessment, for example HAZUS in the USA (Schneider and Schauer, 2006), RiskScape in New Zealand (Schmidt et al., 2011), CAPRA (Cardona et al., 2010), MATRIX (Garcia-Aristizabal and Marzocchi, 2013) and RISK-GIS in Australia (Granger et al., 1999). The common aspect of these tools is that they are used to analyse damages and replacement costs, casualties, disruption and the number of people affected by various hazards. They are also very data demanding. They differ in terms of the methods used for hazard assessment, asset exposure analysis, vulnerability assessment and risk calculation.

Relatively limited work has been carried out on integrated multi-hazard risk assessments for hydro-meteorological hazards in mountainous areas. This is related to the problem that mass movement hazard is particularly difficult to quantify in a medium-scale assessment, due to lack of historical data to correlate triggering events with the associated landslide density, the difficulty to express the intensity of mass movements, and the lack of vulnerability curves for many types of mass movements. Also the interaction between the different types of hazards is complicated, as they may influence each other (e.g. landslides damming streams may lead to flash floods), and they may have very different impacts on the elements-at-risk (Kappes et al., 2010, 2011; Hufschmidt and Glade, 2010; Papathoma-Köhle et al., 2011). There are still no software tools available for the combined analysis of flood and landslide processes (e.g. Gruber and Mergili, 2013). Bell and Glade (2004) developed a raster-based multi-hazard risk analysis approach for snow avalanches, debris flows and rock falls and applied it in an area in Iceland. The final risk to life and economy, expressed as total value at a community level, was obtained by summing the risks due to each single hazard. Marzocchi et al. (2012) carried out a multi-hazard risk assessment in a municipality in Italy, in which they ranked the risk of five types of hazards (volcanic, seismic, flood, landslide and industrial) using the value of annual risk. Van Westen et al. (2014) showed a procedure to quantify multi-hazard risk related to mass movements and flood at a medium scale for the Barcelonnette Basin, French Alps, in which the temporal probability of triggering events for different hazard types (shallow landslides, debris flows, rock falls, snow avalanches and floods) was considered, based on historical hazard events. For the quantification of multi-hazard probability and vulnerability, Ming et al. (2015) applied the copula theory and trend surface analysis to obtain the joint probability distribution in a case study area in the Yangtze River Delta region, China. Although the hazard types were limited and the same vulnerability model was used for different sample areas, the way to quantify the joint return period of different hazards was innovative. A quantitative probability model for evaluating multi-hazard risk was also proposed by Liu et al. (2014), in which hazard loss was not analysed but the interaction effect of different hazard types was evaluated.

Uncertainty is an inherent aspect of multi-hazard risk assessments, and the various components have a large degree of uncertainty, such as the temporal probability of hazard scenarios, the associated distribution and quantification of hazard intensity, the interaction of hazard events, the quantification of elements-at-risk, and the physical vulnerability expressed as a function of hazard intensity and degree of loss. Methodologically, uncertainty can be incorporated into risk assessment using probabilistic methods, such as the application of Monte Carlo simulation generating a large number of possible risk scenarios, resulting in the calculating of a loss exceedance curve (e.g. Grunthal et al., 2006; Mignan et al., 2014; Ming et al., 2015). However, application of such approaches in mountainous environments, involving mass movement hazards in combination with flash flood, is greatly hampered by the lack of data and appropriate models, and the extreme modelling time required.

Therefore, we propose a simpler approach for such environments using a risk curve which is generated using a limited number of scenarios. A risk curve graphically represents losses (economic and casualties) plotted against the annual probability of occurrence of triggering events (Schmidt et al., 2011; Van Westen et al., 2014). Our study aims to provide a methodological procedure for quantitatively assessing multi-hazard risks at a medium scale (1:25,000 to 1:50,000) in mountainous areas prone to hydro-meteorological hazards, such as debris flows, flash floods, and river floods. The method incorporates the deficiencies in available data, and proposes a combination of quantitative models combined with expert-based assumptions to quantify the risk as minimum, average or maximum risk curves. The risk associated with each hazard process is quantified based on its intensity and spatio-temporal probability, the exposed elements-at-risk (buildings and people inside buildings) and their physical vulnerability. The historical hazard events and damage data are used to derive a number of triggering events, with a range of temporal probabilities and with associated hazard maps. The hazard extent and intensity are modelled for these scenarios at medium scale using quantitative empirical and numerical models. Uncertainties in temporal probability, hazard intensity, the value of exposed elements-at-risk and physical vulnerability are determined and expressed as maximum and minimum values. These are used in the risk calculation resulting in three risk curves per hazard type, each representing the minimum, average or maximum risk. The method is schematically presented in Fig. 1.

2. Study area

The Fella River valley is located in the province of Udine, within the Friuli-Venezia Giulia (FVG) region, in the north-eastern part of the Italian Alps (Fig. 2). The Fella River is a major tributary of the Tagliamento River. The study area covers 247 km^2, and comprises four local administrative units: Dogna, Pontebba, Malburghetto-Valbruna, and Tarvisio. The Fella River valley ranges in elevation in this sector between 426 and 2753 m a.s.l. Land cover consists of predominately forested areas (75%), with approximately 10% bare surface and 8% grasslands, with the urban areas located along the valley bottoms and on alluvial fans (Malek et al., 2014). Geologically, the area is underlain mostly by Permian and Triassic formations, consisting of dolomite, limestone and calcareous-marls. Quaternary deposits are mostly represented by debris fans, and glacial and alluvial deposits (Tropeano et al., 2004; Calligaris et al., 2008). The area is also characterized by complex geological structures including folds, faults and fractures which contribute to the instability of slopes. Historically, the Fella River valley is affected mainly by floods and mass movements (Manca et al., 2007).

The catchment has an average annual precipitation of 1920 mm which can reach up to 3000 mm in the higher part of the study area, and extreme daily rainfall exceeding 50 mm has been recorded frequently in the area in a 20 to 30 year time span. Rainfall produced by a convective storm in August 2003 resulted in severe flood and debris flows throughout the Fella River valley. During this event, daily precipitation was between 350 and 450 mm, with most of the rain falling in a 12 h period and reaching peak intensities higher than 100 mm h^{-1} (Sangati and Borga, 2009). More than 100 debris flows were triggered, including an unusually large debris flow occurring in Rio Cucco Village (Malburghetto Commune), with a volume of approximately 78,000 m^3 (Marchi et al., 2009). This event caused loss of life and substantial disruption to the local economy, involving direct damage close to 1 billion euros (Tropeano et al., 2004).

3. Methodology

The methodology proposed in this study follows a number of steps: basic data collection, hazard assessment, generation of elements-at-risk maps, vulnerability assessment, loss estimation and multi-risk estimation (Fig. 3). Different types of data were collected, including environmental conditions, rainfall, historical hazard events and data on the elements-at-risk. Digital elevation data were available in the form of

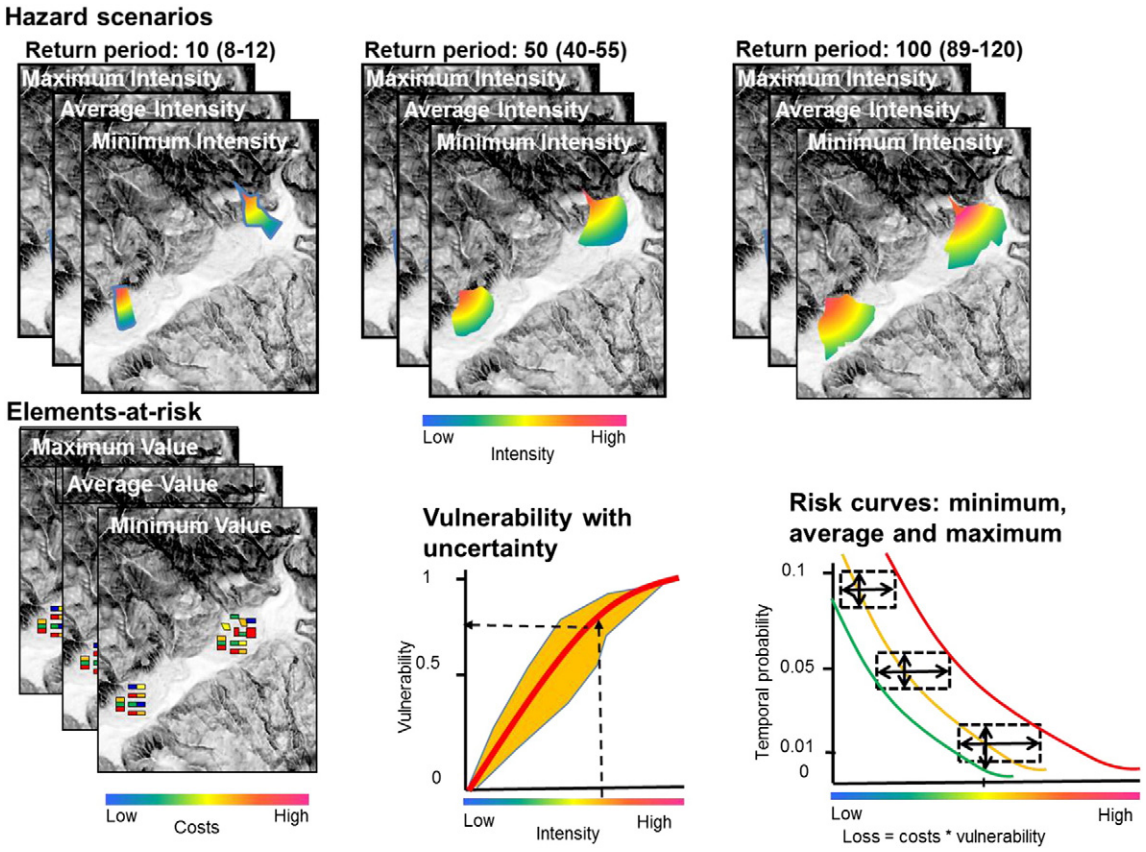

Fig. 1. Schematic representation of the simplified procedure of risk assessment for hydro-meteorological hazards proposed in this research. Different hazard scenarios are defined, and the return periods are represented using the average and range (minimum to maximum). Minimum, average and maximum hazard intensities are modelled for these scenarios. Vulnerability is also indicated with minimum, average and maximum values, as are the values of the elements-at-risk. Finally three risk curves are generated for the minimum, average and maximum data.

two high resolution Digital Elevation Models (DEMs) with 1 m spatial resolution, which were generated from airborn LiDAR data. One of these datasets was available for 2003 and one for 2007, which only covered the areas that were affected by the large debris flow and flood event of 2003.

3.1. Hazard assessment

3.1.1. Historical hazard event inventories

A compilation of historical hazard events was carried out for mass movements and river floods, as a necessary preparatory step for the hazard modelling. Historic mass movement information was collected from web-based archives generated between 1999 and 2011 by the Italian AVI (CNR-IRPI, 2014) and IFFI projects (ISPRA, 2014), the Geological Service of the FVG region and landslide experts at the University of Trieste. The mass movement inventory was checked carefully based on image interpretation using high resolution orthophotos from 2003, and satellite images from several dates over the past 15 years. The collected mass movement inventory maps contain information about the hazard class, type of movement, state of activity and date of occurrence. The detailed image analysis revealed a number of additional mass movements. They were added to the inventory map, which was digitized in GIS.

Although the Fella River valley is affected by many types of mass movements including rotational and translational deep-seated landslides, shallow landslides, earth spreads, rock falls, debris flows and slow moving earth flows, we decided to limit the mass movement risk assessment to debris flows, as these cause the majority of damages to the settlements and infrastructure located along the Fella River valley and the alluvial fans of the tributaries (Fig. 2).

3.1.2. Definition of hazard scenarios

The next step was to create hazard scenarios, which will be later characterized by their frequency and intensity maps, required for the risk calculation. These hazard scenarios were defined based on the return period of the triggering rainfall events for debris flows and flood. Rainfall return periods were estimated through a magnitude–frequency analysis of daily rainfall data.

Using the information on the mass movement types, and date of occurrence from the spatial movement inventory database, we generated separate debris flow inventory maps for each year for the period 1996 to 2011. Since each mass movement polygon contained a description on the mass movement type and the year of occurrence, this could be done using a simple GIS operation. The debris flow polygons include both the initiation areas, the transportation zones, and the accumulation areas. We analysed the rainfall conditions for the events that triggered the debris flows.

Based on the historical mass movement inventories and rainfall events, a number of hazard scenarios were identified. A hazard scenario is a rainfall event with a certain frequency that triggers a certain number of debris flows and flash floods. Rainfall data were collected from eight rain gauges, with daily precipitation available from 1920 onwards. The return periods for different rainfall events were calculated using the Generalized Extreme Value (GEV) distribution (Wilks, 2011). Four hazard scenarios were defined, based on the number of debris flow triggered. For each hazard scenario the variation in the return period was

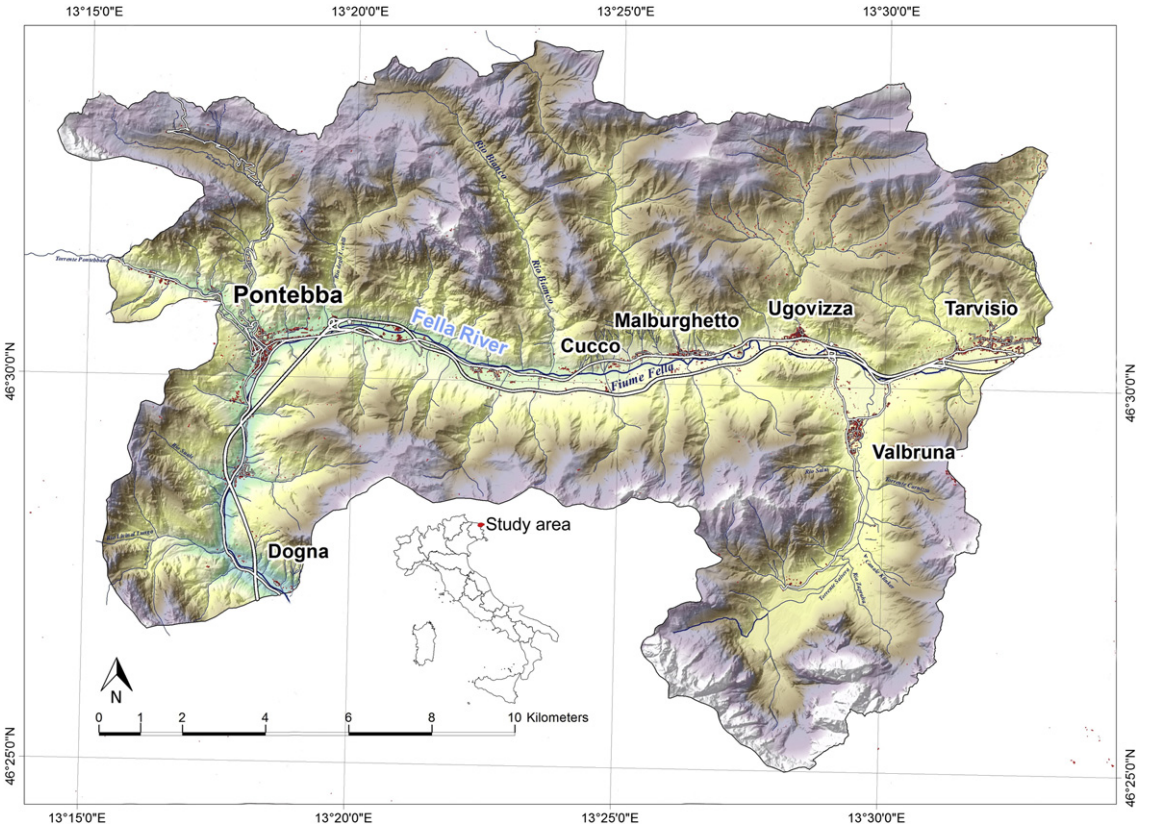

Fig. 2. Location of the study area in the upper part of Fella River valley, NE Italy.

determined and the associated number of debris flows was estimated based on the historical mass movement inventory.

3.1.3. Debris flow hazard assessment

Debris flow hazard assessment consisted of three different components (Fig. 1): first a debris flow initiation susceptibility assessment was carried out, followed by a debris flow run out susceptibility modelling, and finally the generation of debris flow intensity maps. According to a previous study (Hussin et al., 2016), five factor maps (lithology, land-cover, altitude, plan curvature and slope) were collected for the susceptibility analysis of debris flow initiation. The lithological map, available at 1:150,000 scale, was produced by the FVG Geological Service and originally contains more than 35 classes, which were reclassified into eight classes. The land-cover map at 1:100,000 scale was developed by the CORINE land cover project (EEA, 2014) and later updated by the MOLAND project (JRC, 2014). The map with more than 30 classes was generalized to seven classes based on similarities in land cover types. Three factor maps were derived from the DEM and were classified into 10 quantile classes. The quantile classification has been applied in several landslide susceptibility studies (Castellanos et al., 2008; Blahut et al., 2010; Martha et al., 2013) and is useful to proportionately distribute rank-ordered data to better study the influence of factors on landslide occurrence. Debris flow initiation susceptibility assessment was carried out using Weights of Evidence modelling (Neuhauser and Terhorst, 2007; Dahal et al., 2008), with varying sampling methods and different combinations of intrinsic factors (Hussin et al., 2016).

Debris flow run-out modelling was carried out with the Flow-R software (Horton et al., 2013), which uses a GIS-based empirical distribution model to probabilistically estimate the flow path and run-out extent of gravitational mass movements at a regional scale. The modelling procedure consisted of four steps: (1) source area identification; (2) parameterization of the run-out model; (3) run-out modelling and hazard intensity determination; and (4) spatial probability calculation. The areas with the highest initiation susceptibility were selected for the source areas definition. For each hazard scenario, the pixels with the highest debris flow initiation susceptibility, resulting from the statistical analysis, were selected as source areas. In addition, two other criteria sets were used partly based on previous studies (Horton et al., 2008, 2013; Blahut et al., 2010; Kappes et al., 2011). These relate to the planar curvature and to the relation between slope angle and upslope contributing area (Hussin et al., 2014). These criteria were updated specifically for the Fella River valley.

Two parameters were required to model the run-out with Flow-R: the minimum travel angle and the maximum velocity. These two parameters were estimated with minimum, average and maximum values, based on a number of back-calibrated historical debris flows, using the physically-based Flo-2D software. The output of the Flow-R model was in the form of two maps, one representing the kinetic energy and the other showing the relative probability of the debris flow reaching the location. The relative probability values were subsequently converted into debris flow height which was used later in physical vulnerability quantification. An empirical transfer function from probability to height was generated by comparing quantile classified Flow-R probability maps with back analysed debris flows heights from the physically based Flo-2D software. The detailed method is explained by Hussin et al. (2014). The modelled debris flow run-out areas were larger than the actual areas that were affected based on the historical inventory. All debris flow areas that are part of the historical inventory were given a spatial probability of 1, which includes modelled areas that overlap with the historical events. The spatial probability of the simulated debris flows that do not overlap with past events, were calculated by dividing the total area of the historical events of a given return period scenario by the total area of the modelled debris flows of that scenario.

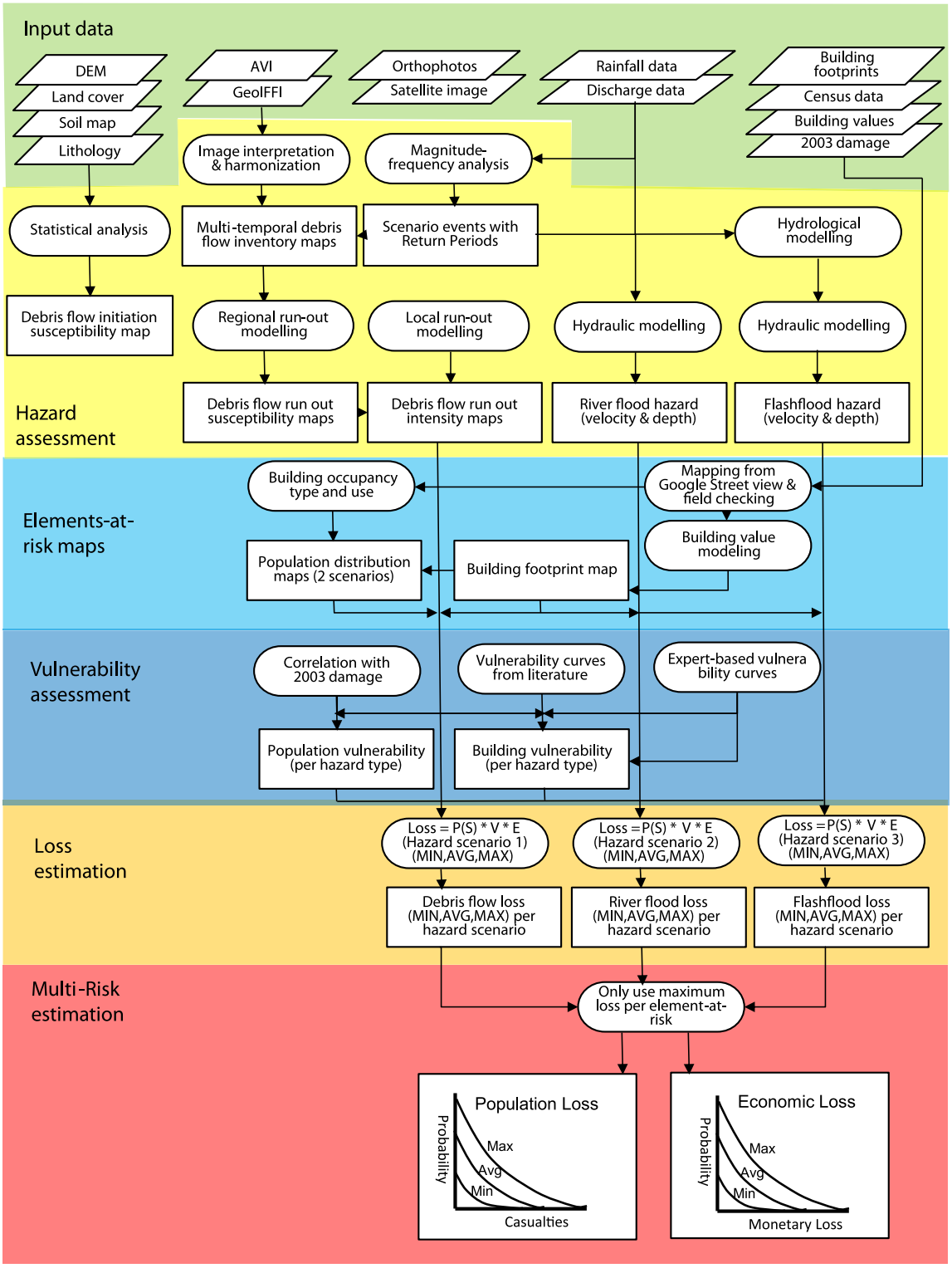

Fig. 3. Methodology for multi-hazard risk assessment in the Fella River valley, Italy.

3.1.4. Flash flood hazard modelling

To model the flash flood intensity in the tributaries of the Fella River for the hazard scenarios, we applied a spatial hydrological runoff and erosion model, OpenLISEM, capable of modelling shallow floods in rural and urban areas. The OpenLISEM is a freely available process based modelling software (Jetten, 2013), which handles both sediment and hydrological processes. OpenLISEM is an event-based model, which models the surface runoff during and immediately after a rainfall event. Evapotranspiration and groundwater movement are not simulated. It models the hydrological processes of infiltration and runoff in detail with time steps of < 1 min and grid sizes of < 1 ha. Infiltration is modelled using the principles of Green and Ampt (1911). The method uses saturated hydraulic conductivity (K_{sat}), the total pore volume, the soil storage of the top layer and the suction of the soil. The infiltration rate (in

mm h^{-1}) at the soil surface is calculated following the Law of Darcy, where the suction exerted by the soil, and the distance from the surface over which the suction is applied are important factors. OpenLISEM simulates three flow processes: overland flow over the entire flow network, channel flow with a separate channel network using a number of maps that define the channel dimensions, and simulated floods when the channels overflow.

OpenLISEM makes use of input maps generated in the PCRaster environmental modelling software (Karssenberg et al., 2010). It includes various attributes of land cover, such as cover type, canopy storage, surface roughness and Manning's n values for flow resistance. It uses soil texture classes with pedotransfer functions for the soil attributes indicated above. It also requires a network of local surface drainage direction and outlet points. Moreover, it also needs channel parameters such as channel direction, width, and gradient. The model generates output maps of total infiltration, interception, runoff fraction, a runoff map and an error report. In addition it gives discharge at the outlet points of the sub-watershed which needs to be pre-defined by the user. Since the discharge is calculated at every time step (pre-defined) it is possible to generate a hydrograph. At the end of the model run, it also shows a hydrograph and the water depth distribution. In this study, rainfall data from the Pontebba and Malburghetto-Valbruna rain gauge stations were used for describing typical events characterized by the hazard scenarios, mentioned in Section 3.1.2.

3.1.5. River flood hazard modelling

To model the river flood hazard of the main Fella River, a hydrological study of the area was carried out followed by a hydraulic modelling for different possible discharges associated with the return periods. The hydraulic modelling for flood mapping was performed using HecRAS 4.1 and its GIS-assisted version GeoHecRAS (ArcGIS 10.1). The bathymetry of the river and corresponding topography of the flood plain was obtained from the LiDAR data at 1 m resolution. Due to the high computational demands of the model, the river was divided into two sections: the Northern corridor, running East–West from Ugovizza to Pontebba, and the Middle corridor, running North–South from Pontebba to Dogna (Fig. 2). The model showed a river regime which was mainly supercritical with rapid flows and high shear forces. Model outputs included flood boundaries, inundation depths, and velocity and stream power maps for discharges ranging from 100 to 700 m^3/s (at Pontebba). Sources of difficulty for the modelling included the large amount of roads, railways and highway intersections affecting the LiDAR data accuracy and the flow behaviour, and the sinuosity of the river bed as a limitation for a 1-D hydraulic model. Based on the above process, flood boundaries, water depth, and velocity maps were obtained for the hazard scenarios through hydraulic modelling with HecRAS.

3.2. Elements-at-risk database

This study focuses on risk posed by hydro-meteorological hazards to residential buildings and people inside these buildings. A database of elements-at-risk was created based on an existing building footprint map provided by the Civil Protection of the FVG Region, which was generated before the 2003 disaster.

Detailed image analysis was carried out using the available orthophotos, Google Earth and Google Street View, during which it was possible to update the map by removing the buildings that were destroyed or abandoned in 2003, adding new buildings, and classifying the buildings on the basis of their occupancy type, construction type and number of floors. Field work was carried out to validate the remote-desktop mapping results.

In order to express the risk in monetary values, data on the value of buildings were obtained from the Italian Revenue Agency (Agenzia delle Entrate, 2013) for the second semester of 2013. These data were given per cadastral zone, as minimum and maximum standard price (€ m^{-2}) for different building occupancy types. The building market value was calculated by multiplying the minimum and maximum standard price with the total building area. From this information an average market value was also determined.

Population data at building level were unavailable; however, the total number of people in each commune was known (ISTAT, 2014) and used together with the building information (occupancy type, area and the number of floors), to calculate the average number of people per residential building by applying a dasymetric mapping approach. Only residential buildings were used for estimating the spatial distribution of people in the study area. Given the specific economic activities in the region and the large number of holiday houses, two scenarios were taken into account: a non-tourist season scenario, where most of the population is located in the residential buildings and a tourist season scenario, where also additional population is distributed over hotels and other tourist accommodations.

3.3. Vulnerability assessment

Physical vulnerability is defined as the expected degree of loss for a building or person inside the building, as a consequence of an impacting hazard of a given intensity (Hollenstein, 2005). The resulting vulnerability value ranges between 0 (no damage) and 1 (total damage). Because the degree of loss must be expressed quantitatively in order to calculate the economic loss and risk to life, vulnerability curves were generated for buildings and population, taking into account debris flow height (in m) and water depth (in m).

Three methods were used for generating vulnerability curves: collection of existing curves from literature, expert-based generation of curves, and correlating the damage with the intensity for the 2003 event (Fig. 3). We compared vulnerability curves for debris flows derived in the Italian Alps (Akbas et al., 2009; Quan Luna et al., 2011), South Tyrol, Italy (Papathoma-Köhle et al., 2011; Eidsvig et al., 2014) and East Tyrol, Austria (Fuchs et al., 2007). Eidsvig et al. (2014) analysed the uncertainty of vulnerability curves for debris flows, and suggested to develop either an uncertainty range in the curves, or to develop fragility curves which represent the probability of a certain damage state being exceeded. We decided to select the uncertainty band approach indicating the curves as minimum, average and maximum curves, as this was easier to understand and to develop using expert opinion. For population vulnerability in relation to debris flows there is much less information available in the literature. Li et al. (2010) present an overview of work done on this topic, and differentiate between direct and indirect estimation of population vulnerability, where the latter is made as an empirical relation between the damage state of a building and the probability of injury. Vulnerability of people to landslides was also studied by Finlay (1996) and Ragozin and Tikhvinsky (2000). Examples of uncertainty analysis related to vulnerability assessment are given by Merz and Thieken (2009), and specifically for landslides by Uzielli and Lacasse (2007); Kaynia et al. (2008) and Totschnig and Fuchs (2013). For flood, more literature is available on vulnerability curves for buildings and population from different environments and for different types of buildings (e.g. USACE, 2000; Dutta et al., 2003; Penning-Rowsell et al., 2005; Jonkman et al., 2008; Reese and Ramsey, 2010). Godfrey et al. (2015) also used such a literature survey to generate a generic set of vulnerability curves, using the range of values to express the level of uncertainty. For those areas where actual damage information was available for the 2003 disaster event, we generated vulnerability curves by relating the estimated debris flow intensity with the degree of loss. The latter was defined as the ratio between building damage and market value. The building market value was calculated using the Italian Revenue Agency data. The damage costs as well as photo-documentation of damaged buildings were available from the Civil Protection of FVG Region only for a limited number of structures (in the Malburghetto-Valbruna commune). Therefore, we also used vulnerability curves from literature and expert knowledge of engineers and geologists to generate vulnerability curves by relating debris flow

deposit height or water depth with degree of damage. A comparable (expert-based) approach was applied for vulnerability of people located in buildings.

3.4. Loss estimation

Losses were calculated using the following equation:

$$L = P_s \times E \times V \quad (1)$$

In which P_s = the spatial probability that a particular pixel in the susceptible areas is affected given a certain hazard scenario k; E = the quantification of the amount of exposed elements-at-risk, given a certain hazard scenario k (e.g. expressed as monetary value or number of people); V = the vulnerability of elements-at-risk given the hazard intensity under the specific hazard scenario k (Fig. 3). In the case of buildings the quantification was given as the monetary value of the exposed buildings, and in the case of population it was given as the number of persons within a building, given one of the two population scenarios for tourist and non-tourist seasons.

We used a total of 36 different hazard maps, representing three hazard types (debris flows, river flood and flash flood), modelled for four hazard scenarios, and with each scenario simulated using the minimum, average and maximum intensity values. The exposure of buildings was calculated by overlaying the hazard maps and the building footprint map. For each building the hazard intensity was recorded for each of the hazard maps (e.g. average debris flow intensity for a moderate event). The intensity was then converted into vulnerability by selecting the appropriate vulnerability curve for the given hazard process, and construction type of the building. Finally the minimum, average and maximum loss for each combination of hazard type, elements-at-risk type, and hazard scenario was calculated by multiplying the vulnerability with the monetary value (in case of buildings) or with the number of people (in case of population). The entire procedure was automated using so-called script files in a Geographic Information System (ITC, 2015). The losses are given for each individual building polygon.

3.5. Multi-hazard risk estimation

The last step in the analysis was to integrate the results of the loss estimation into a multi-hazard risk estimation, integrating the risk for the different hazard types, hazard scenarios with different return periods, and their variations (minimum, average and maximum). The multiplication of spatial probability, exposure and vulnerability (Eq. 1) should be done for all elements-at-risk for the same hazard scenario. Since we consider three types of hydro-meteorological hazards (debris flows, river floods and flash floods) that are dependent on the same triggering event, an element-at-risk (e.g. a building) which is damaged by one of the hazard types might also be affected by another damage type during the same triggering event. Considering that one building may be simultaneously impacted by more than one type of hazard (e.g. flash flood and debris flow), the maximum loss, and not the sum of all losses per building is taken into account. This is done for each building in the study area and the resulting losses for all buildings in the study area are summed up, and plotted in the risk curve against the annual probability of occurrence of the hazard-scenario, which is calculated as the reciprocal of the return period in years. This is repeated for all available hazard scenarios. At least three individual hazard scenarios should be used, although it is preferred to use at least six events with different return periods to better represent the risk curve. The area under the curve is then calculated by integrating all losses with their respective annual probabilities, which gives the average annual loss (Figs. 1 and 3).

The uncertainty is taken into account within each step of the analysis, and in this research we represented each factor (P_S, E and V) with a range of values (minimum, average and maximum). These were either calculated or modelled, but were also determined based on expert opinion when not enough information was available to actually calculate them.

4. Results

4.1. Debris flow inventory

After compiling all available mass movement inventory data, and after careful checking through image interpretation, the mass movement database was generated which consisted mainly of debris flows, rock falls, and shallow landslides. Most of the rock falls and debris flows occur in the uninhabited higher parts of the study area, while the populated areas are affected mainly by debris flows. The inventory contained a total of 408 debris flows, with GIS point-data indicating the location of the top of the debris flow scarps and polygon-data of the debris flow runouts, which include the debris flow transportation and deposit zones. Table 1 provides information on the debris flow activity in the period 1996—2011, with the highest numbers and areas reported in 1996 and 2003.

4.2. Definition of hazard scenarios

In order to classify the events listed in Table 1 into hazard scenarios with associated return periods, an analysis of rainfall was carried out. We collected data from eight rainfall stations of which three stations are located within the study area (F–1, F–4 and F-5 in Table 2) and five in the surroundings. In the past 20 years the records have undergone validation by the Italian Hydrographic Service, which included checking the stations with neighbouring stations as well as annotating the records.

The cumulative frequency distribution (CDF) for annual daily maximum precipitation was assessed. The CDFs can be related to the return period for precipitation amounts, estimating the average recurrence interval between events of a similar magnitude. The CDF extreme daily precipitation events were calculated both empirically and using the Generalized-Extreme Value distribution (GEV). GEV is based on the theory that the largest values from the same distribution will follow a known distribution, which does not depend on the original distribution (Wilks, 2011), and is frequently used for precipitation annual maxima (e.g. Buonomo et al., 2007).

Fig. 4 displays the return periods for annual maximum 1-day precipitation for each station, with a solid line for the empirical distribution and a dashed line for the best fit GEV-distribution. Steep curves indicate little increase in precipitation for increasing return periods, while a more gradual curve indicates a faster precipitation increase with an increasing return period. Station F-5, Pontebba, located in the centre of the study area, shows moderate precipitation values for high frequency events, but one of the highest precipitation amounts for low frequency

Table 1
Number and area of recorded debris flows in the Fella River valley for the period 1996—2011. No debris flows were recorded in the missing year in the list.

Year	Recorded debris flows	
	Number	Area (km^2)
1996	137	2.021
1998	13	1.924
1999	6	0.008
2000	8	0.014
2003	144	6.792
2005	8	0.071
2006	30	0.727
2007	38	3.969
2010	13	1.574
2011	11	0.620
Total	408	17.90

Table 2
Overview of climate records for the Fella River valley. Length of rainfall station records for each station is indicated, and the annual total rainfall mean and maximum, as well as the annual daily mean and maximum rainfall.

Station code	Name	Elevation (m a.s.l.)	Rainfall records	Mean annual total (mm)	Maximum annual total (mm)	Mean annual daily maximum (mm)	Maximum annual daily maximum (mm)
F–1	Tarvisio	725	1923–2011	1506	2114	81.0	126.8
F–2	Valico de Fusine	850	1971–2003	1440	1852	81.5	178.5
F–3	Cave del Predil	897	1927–2006	2062	2968	133.0	246.0
F–4	Malburghetto	733	1922–2011	1533	2170	97.0	186.2
F–5	Pontebba	568	1920–2011	1814	2840	126.8	278.6
F–6	Chiusaforte	400	1920–2005	2066	3006	152.6	229.7
F–7	Resia	469	1920–2011	2460	3594	195.1	355.0
F–8	Moggio Udinese	310	1935–2005	1840	2940	138.5	276.6

events. The difference between the empirical and GEV distributions for extreme values highlights the difficulty in determining return periods for extreme events. For all stations, the difference between the empirical and fitted distributions was small (<5 mm) for return periods less than three years, with differences increasing to up to 40 mm for return periods greater than 20 years.

We were not able to classify hazard scenarios purely based on statistical analysis, due to the lack of accurate information on the date of debris flow occurrence or missing rainfall data for some stations. For many debris flow polygons in the database only the year is known which makes it difficult to link them to a specific rainfall event. Therefore, we made an expert-based assessment supported by the statistical analysis of the rainfall and debris flow data, and the four hazard scenarios were identified: major, moderate, minor and frequent. For each of these scenarios, we selected a characteristic debris flow triggering event from the mass movement database, and used the number and area of associated debris flow based on the information from Table 1. Also based on the GEV distributions and their variations, ranges of return periods were determined for each hazard scenario (Table 3 and Fig. 4). The major hazard scenario has the largest number of debris flows, covering the largest areas, and with a large range in return periods, due to the high uncertainty given the relatively short period of the climate record. This hazard scenario is characterized by the 2003 event. The moderate hazard scenario is characterized by the 1996 event, which seems to have almost as many debris flows as the 2003 event, although covering a much smaller area. This may be because the debris flow recording started in 1996, and many of the debris flows attributed to 1996 may have been actually older. The range of area covered by debris flows was more important for defining the class boundaries than the actual number of debris flows, as the area is used later in estimation the spatial probability that modelled debris flow areas might actually be affected during a hazard scenario. The minor hazard scenario is characterized by the inventory from the 2011 event. We also included a frequent hazard scenario, which occurs very regularly, but has a very low number of debris flows and area affected. Fig. 5 shows the debris flow inventories of the representative years for the four hazard scenarios.

4.3. Debris flow intensity analysis

After defining and characterizing the four hazard scenarios, the next step was to generate debris flow susceptibility maps for each scenario. Debris flow initiation susceptibility maps were modelled using the statistical Weights-of-Evidence (WofE) methodology (Bonham-Carter et al., 1988). Weight values were calculated for each factor using the Arc-SDM for tools ArcGIS 10 (Sawatzky et al., 2009). One susceptibility map of debris flow initiation was produced for each hazard scenario using the representative debris flow initiation points (Fig. 6). The resulting four susceptibility maps were classified into five classes ranging from very low to very high. The best performing susceptibility map was for the "major" hazard scenario (Fig. 5) and has an accuracy of 89.2%, based on the area under the success rate curve (Neuhauser and Terhorst, 2007).

For the generation of the debris flow run-out maps, we used only the very high susceptible areas from the debris flow initiation susceptibility maps. We added a criteria to limit the source areas even more, as initial runs with the Flow-R model showed realistic results when using the entire very high susceptible areas. We restricted the debris flow source areas by using only the very high susceptible areas that have a curvature lower than $-4/100\ m^{-1}$ and slope steepness above 15° and an upslope contributing area of 2.5 km^2 or more (Rickenmann and Zimmermann, 1993; Heinimann et al., 1998; Horton et al., 2013). We used the regional scale empirical run-out model Flow-R to generate minimum, average and maximum run-out maps for the four hazard scenarios defined

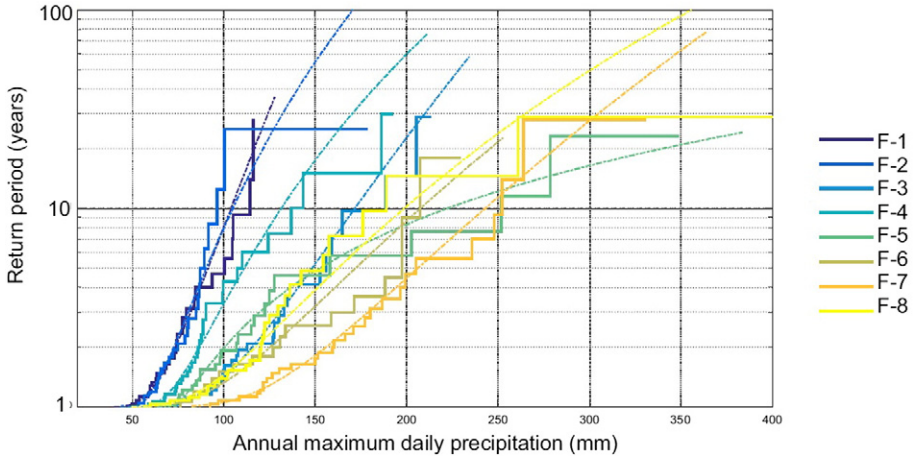

Fig. 4. Annual maximum daily precipitation values for the eight stations in and around the Fella River area. The stair plots show the empirical return periods, while the dashed line plots the best fit GEV-distribution. The stations F–1, F–4 and F–5 were used for determining the range in return periods shown in Table 3.

Table 3
Hazard scenario classification, with associated return periods, representative events from the debris flow inventory shown in Table 1 and the associated number and area of debris flows.

		Hazard scenario			
		Major	Moderate	Minor	Frequent
Return period (years) (with 80% confidence bound)		100–500	25–100	10–25	1–10
Representative events	Year	2003	1996	2011	2005
	Daily rainfall (mm)	354.6	192.2	154.4	90.0
	Return period (years)	133	26	14	8
Historical years used for range of debris flow density		2003, 2007	1996, 2007	2006, 2010, 2011	1999, 2005
Recorded debris flows	Number	38–144	30–137	11–30	6–8
	Area (km^2)	3.9–6.8	2.0–3.9	0.6–1.6	0.008–0.071

earlier. Table 4 shows the model parameters used to produce the run-out maps for each hazard scenario.

The Flow-R run-out model provides output maps that show the probability that a pixel may be affected by debris flows but not the debris flow height itself which is required as intensity input for vulnerability assessment. To transfer Flow-R run-out probability values to debris flow height at a regional scale, the relationships between debris flow height and run-out probability were statistically analysed. For this purpose, we selected a sample of five debris flows that occurred during August 2003 event, located in the most affected area between Cucco and Malburghetto (Fig. 2), and for which we were able to obtain data on the initiation and deposition volumes. We carried out a back analysis for these five debris flows with 5 m resolution data using the Flo-2D local scale physically-based run-out model. The output of the Flo-2D model was in the form of flow depth maps which were overlain in GIS with the Flow-R run-out probability maps. A significant correlation was found between the 10 quantile probability classes and flow depth with an R^2 value of 0.84. We use the established relation to convert the four probability maps at regional scale into debris flow depth maps. Fig. 7 shows the debris flow height maps for the major, moderate and minor hazard scenarios.

The modelled debris flow run-out maps (Fig. 7) contain many more possible run-out areas as compared to the historical debris flow inventories (Fig. 5). The chance that a particular area modelled as debris flow run-out zone would actually be hit by a debris flow during a hazard scenario was estimated using the spatial probability (Table 4). The spatial probability map for each hazard-scenario was calculated by dividing the area of the representative historic debris flow inventories (Table 3 and Fig. 5) by the area of the modelled Flow-R run-out area.

4.4. Flood modelling

Flood modelling was done separately for flash flood of the tributaries of the Fella River, using the OpenLISEM model, and for flood of the Fella River itself using HecRAS. Also here modelling was carried out for the four hazard scenarios. For each hazard scenario, minimum, average

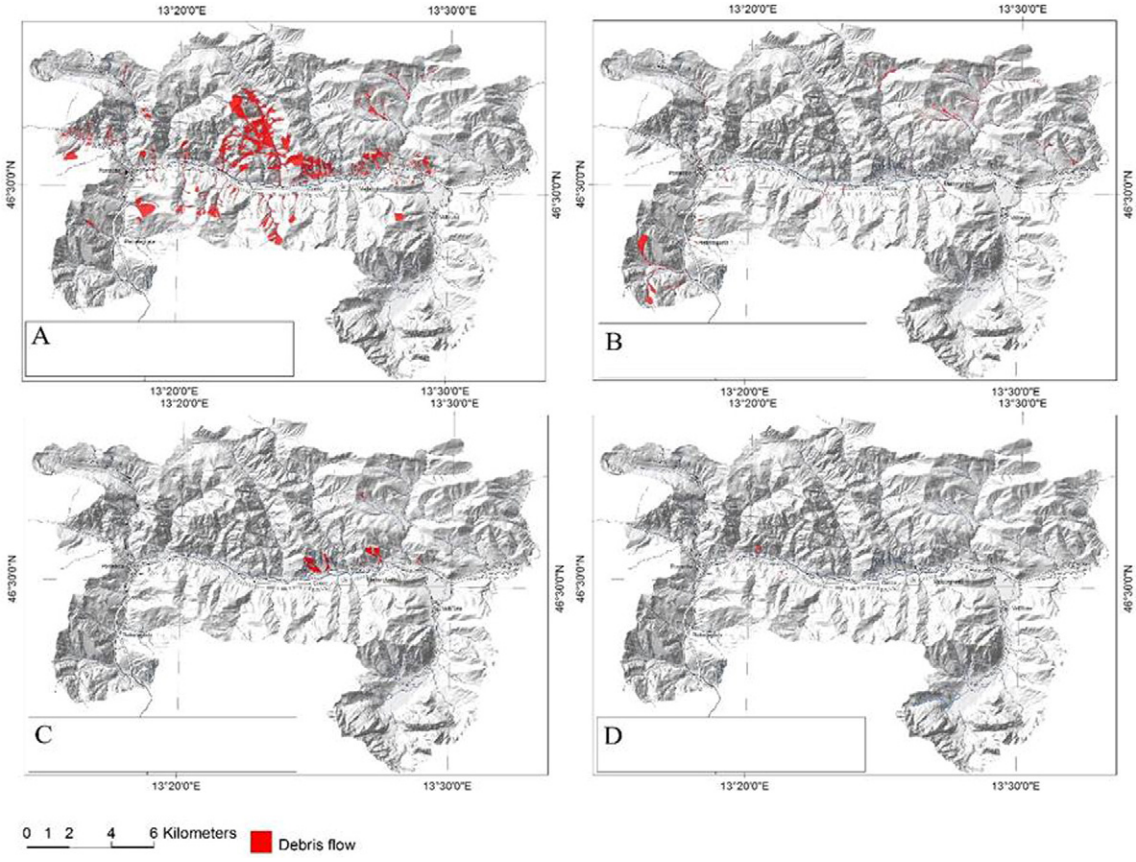

Fig. 5. Representative debris flow inventories for the four hazard scenarios defined in Table 3. A) Major hazard scenario, characterized by the inventory from the 2003 event; B) moderate hazard scenario, characterized by the inventory from the 1996 event; C) minor hazard scenario, characterized by the inventory from the 2011 event; D) frequent scenario, characterized by the inventory from 2005.

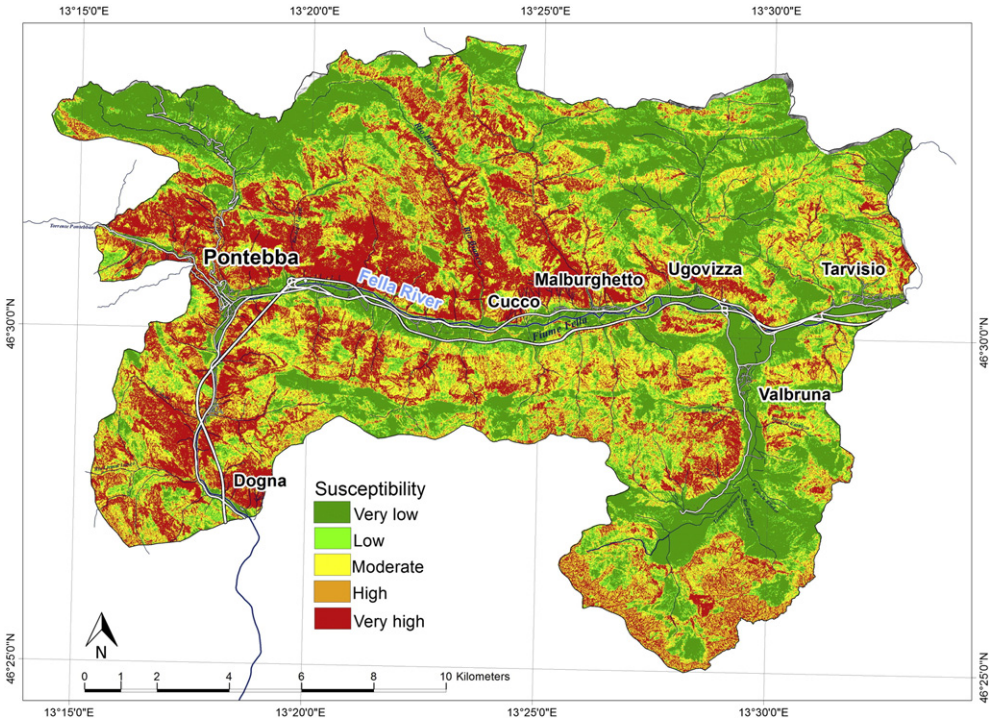

Fig. 6. Debris flow initiation susceptibility map for the major hazard scenario.

and maximum water depths and flow velocities were calculated. Fig. 8 shows the output for modelling the flash flood using OpenLISEM for the major hazard scenario, during which the rainfall event of August 2003 was used as input. The flood areas are mainly concentrated on the eastern and southern parts of the Fella River valley (Fig. 8).

For the flood modelling of the Fella River, a rainfall characterization was implemented using the long-term historical series of the rainfall stations. Despite the availability of information related to land use, topography and meteorological parameters, a rainfall–runoff model was impossible to implement due to the poor records of discharges available in the main stream and the tributaries. Long series of water levels exist at different hydrometric stations, but the data cannot be straightforwardly correlated with discharges due to the high temporal geomorphological variability of the river bed. A frequency analysis of discharges was performed at the Donga catchment outlet given the available 3-years of hourly discharges (2006–2008) provided by the FVG Region. Analysis of the base and superficial flows of such discharges confirmed previous conclusions on the basin hydrological behaviour, according to which most of the rainfall results in base flow (up to 65% of the annual flow) with quick flow mainly occurring during extreme events and antecedent soil moisture determining the flood response. An attempt to implement the HBV model (a semi-distributed hydrologic model to simulate catchment runoff) was made but resulted in poor calibration due to short data series of discharges. In order to determine the return period of modelled discharges, the storms recorded at the Dogna catchment that resulted in quick flow at the main channel were correlated with the peak discharges during the 3-year hourly data. The frequency of the same storms obtained from the long historical series of the same station was finally assigned to the peak discharges in order to provide a return period for the flood analysis. Such return periods are only valid for the catchment outlet at Dogna and a proportional flow based on the drainage area of every sub-catchment was modelled for flood mapping purposes along the main river channel from Ugovizza to Dogna (Fig. 2). The lack of available rating curves or direct measurements of discharges introduced high uncertainty to the frequency analysis of the floods and therefore the results should be considered with caution. The resulting discharges for the hazard scenarios are shown in Table 5.

The hydraulic modelling for flood mapping was performed using HecRAS 4.1 and its GIS-assisted version GeoHecRAS. Model outputs shown in Fig. 9 include flood boundaries, inundation depths and flow velocities for discharges related to hazard scenarios (Tables 3 and 5).

Table 4
Parameters used for run-out modelling.

Hazard scenario		Travel angle (degree)	Velocity (m/s)	Spatial probability
Major	Max.	13	15	0.245
	Min.	15	10	0.131
Moderate	Max.	15	10	0.131
	Min.	18	8	0.050
Minor	Max.	17	8	0.050
	Min.	20	8	0.006
Frequent	Max.	20	5	0.006
	Min.	22	4	0.001

4.5. Buildings and population database

After updating the existing building footprint map through image interpretation of Google Earth and Google Street View images and field checking, a digital building footprint map was generated for the study area, which contains 4778 buildings, with attributes related to occupancy type, construction type, and number of floors. The buildings were classified into 16 occupancy types and six construction types (Fig. 10).

For each building in the database, minimum and maximum market values were calculated using the method described earlier. The results are shown in Fig. 10 for a small part of the study area. The number of persons per residential building and seasonal population scenario were also calculated. The results show that in the communes of Malburghetto, Pontebba and Tarvisio, the population increases significantly in the tourist season compared with the non-tourist season, whereas in Dogna the number of people remains constant for both population scenarios. The spatial distribution of people per building during tourist season is also presented in Fig. 10.

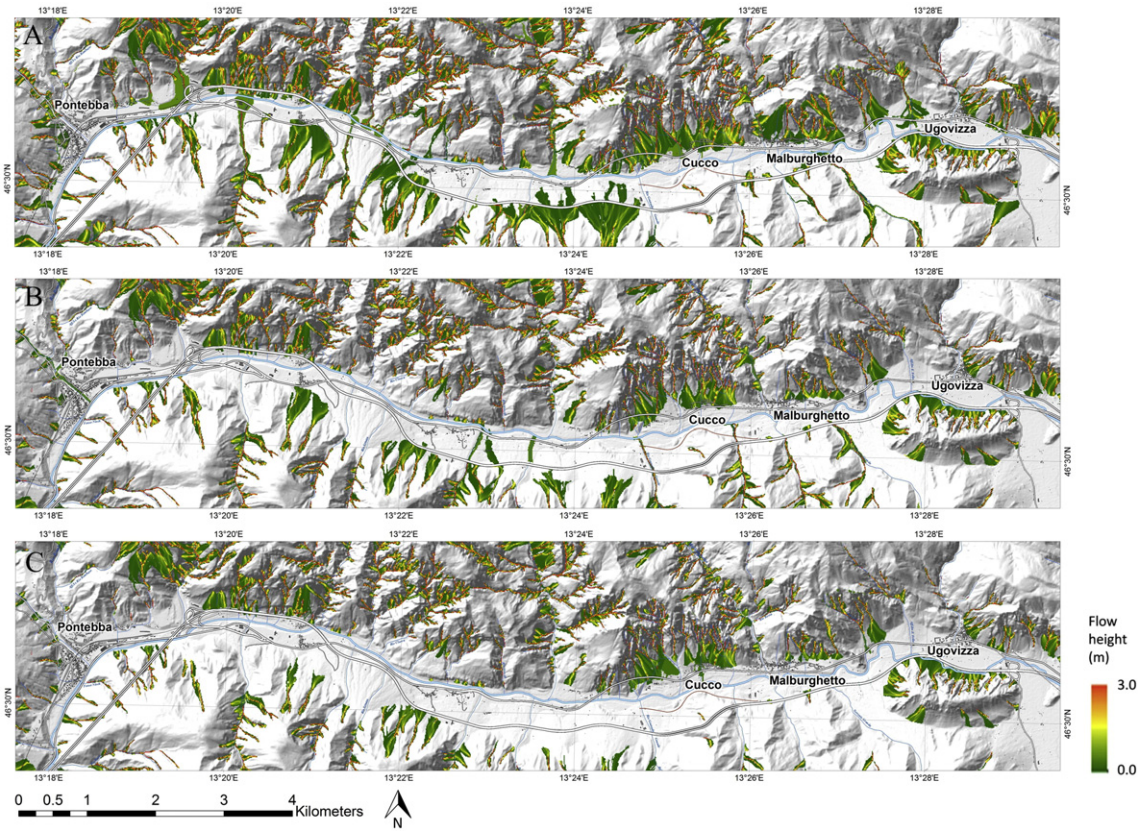

Fig. 7. Shaded relief maps with the maximum debris flow heights for the central part of the Fella River valley between Pontebba and Ugovizza. A) Major hazard scenario; B) moderate hazard scenario; C) minor hazard scenario.

4.6. Vulnerability assessment

We made an inventory of vulnerability curves from literature for floods and debris flows (Godfrey et al., 2015). However, for several of the combinations of construction type and number of floors no vulnerability curves were available from the literature.

For those locations where damage information was available from the 2003 disaster in the Fella area, we tried to correlate this with the

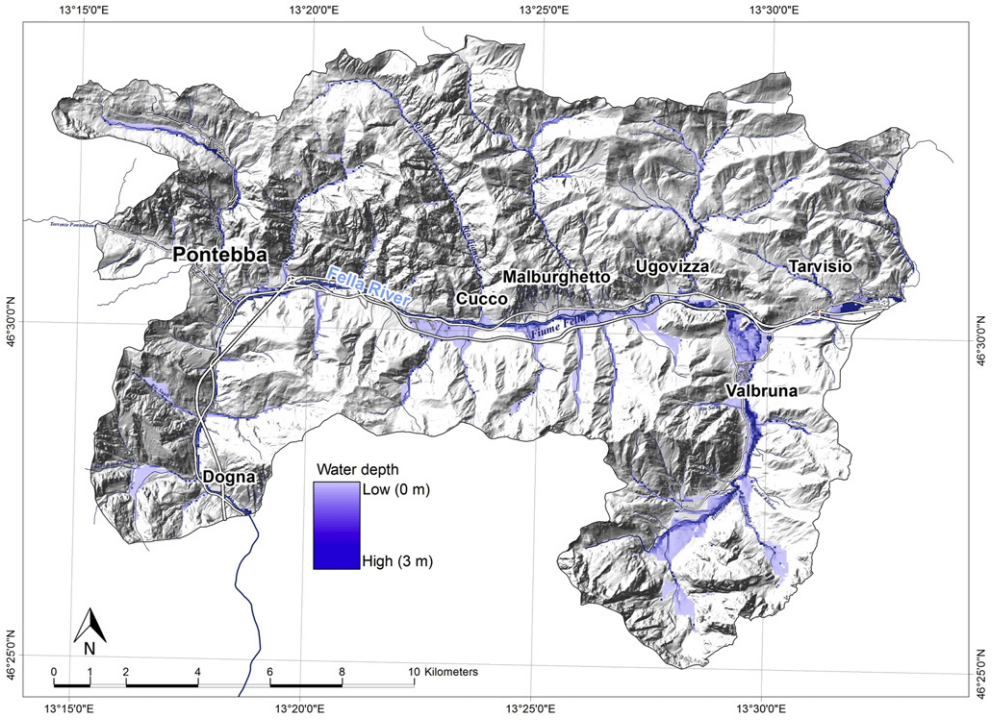

Fig. 8. Flash flood water depth distribution modelled for major hazard scenario (event 2003).

Table 5
Estimation of return periods for discharges at Dogna based on 2006–2008 daily data.

Hazard scenarios		Return period (years)	Estimated peak discharge in Dogna (m^3/s)
Major	Min.	100	882
	Max.	500	1029
Moderate	Min.	25	588
	Max.	100	735
Minor	Min.	10	441
	Max.	25	500
Frequent	Min.	1	294
	Max.	10	300

modelled hazard intensities. Papathoma-Köhle et al. (2012) developed a method for estimating vulnerability of buildings to debris flows based on detailed documentation of damaged structures. This approach was adopted in this study. The height of the debris flow deposits for a specific building was either measured from the run out modelling results of Flo-2D for the five sample debris flows mentioned before, or estimated by analysing a set of field photographs acquired shortly after the event by the Civil Protection of FVG Region. The damage data, representing the compensation offered by the government after the event, were provided by the municipality of Malburghetto. The damage ratio was calculated by dividing these by the building costs modelled (Fig. 10).

We developed the vulnerability curves for building construction types (wood, masonry and concrete) which we combined with the number of floors. Two sets of curves were made: one set for physical vulnerability of buildings, and the other for population vulnerability. The first set of curves represents the relation between the hazard intensity and the degree of damage for the building and its contents. We included also the contents of buildings into the vulnerability curves, as content damage is often more severe in flash floods and low magnitude debris flows, which often do not destroy a building, but inundate it and damage the contents. The vulnerability therefore increases with increasing height, especially for the first meter, as most of the furniture and equipment are damaged on the first floor. Population vulnerability curves were made for people inside of buildings, and are therefore also

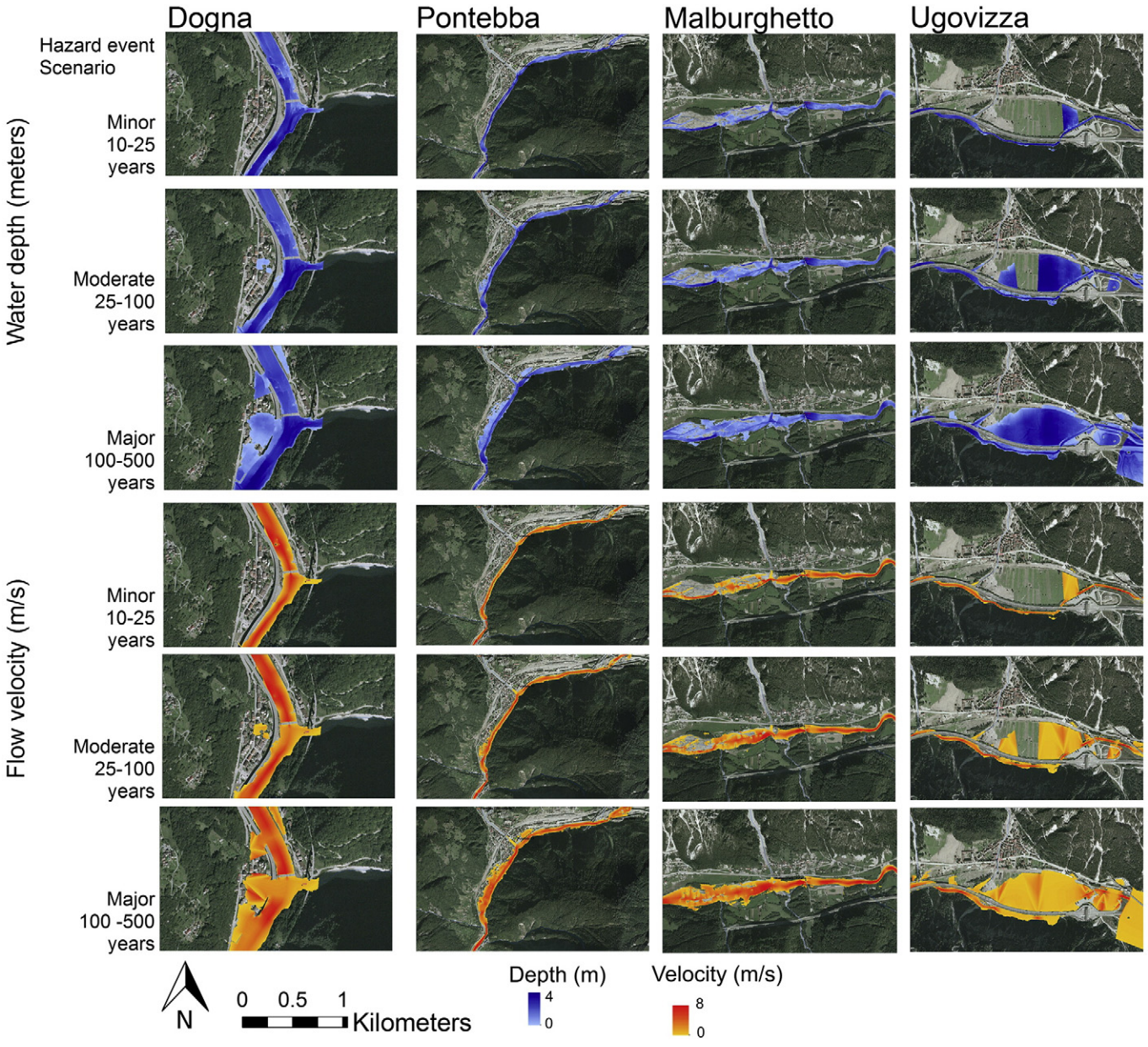

Fig. 9. Flood depth and velocity maps for three hazard scenarios and four locations (Fig. 2).

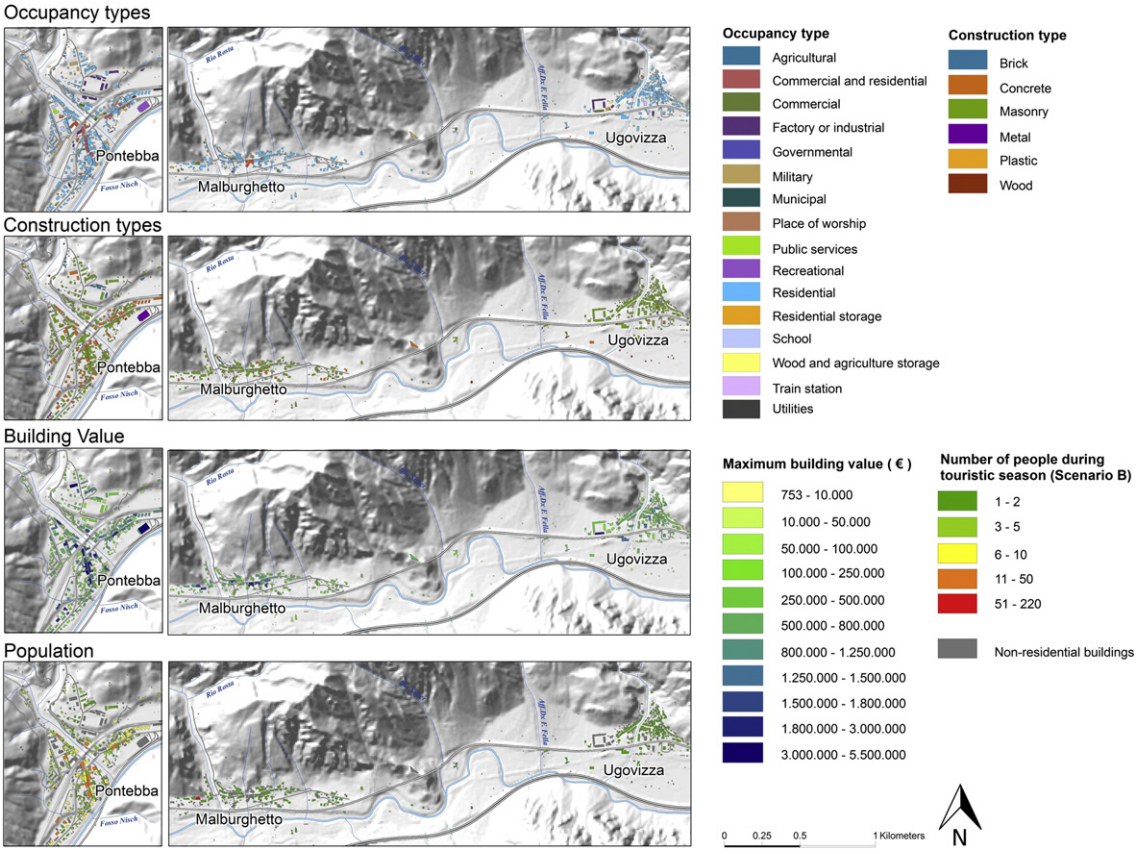

Fig. 10. Maps of four main building attributes for some selected areas around Pontebba, Malburghetto and Ugovizza: occupancy types, construction types, building values and number of people per building during the tourist season.

linked to the same building classification as the physical vulnerability curves. The population vulnerability curves express the chance that a person will be severely injured or killed given the intensity of the hazard. As most of the mountain hazards which we evaluate in this research occur instantaneously, we do not take into account the evacuation of people to other locations. We do take into account that people can move to higher storeys within the building in case of flood, if more than one storeys are available. That is why we consider much higher

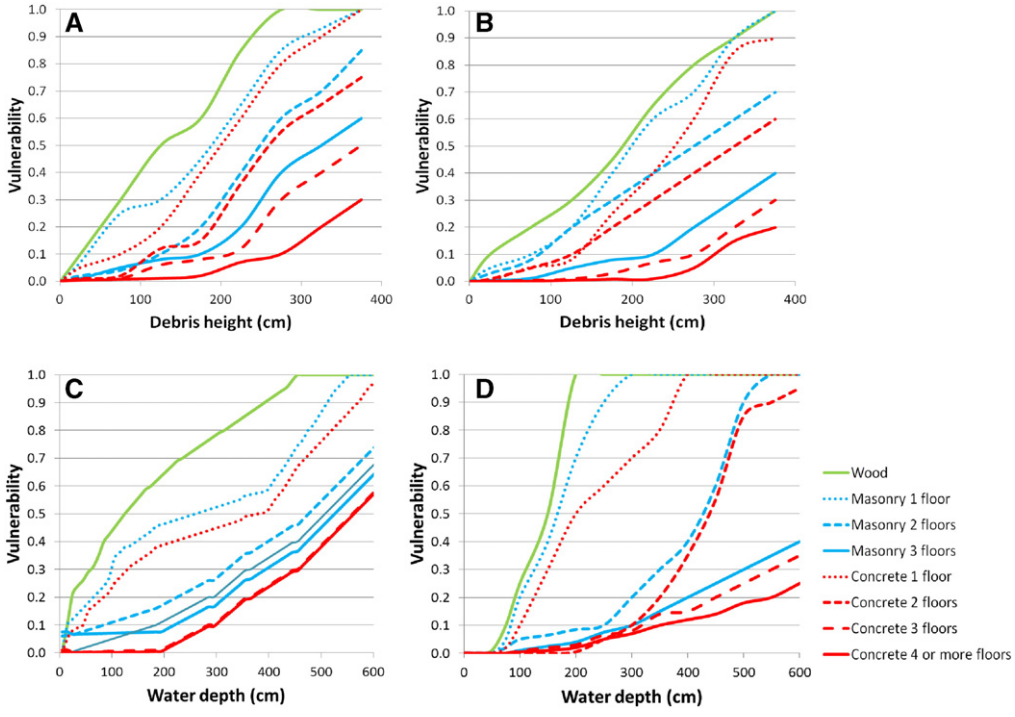

Fig. 11. Average vulnerability curves for debris flows (A – for buildings, B – for people) and floods (C – for buildings, D – for people).

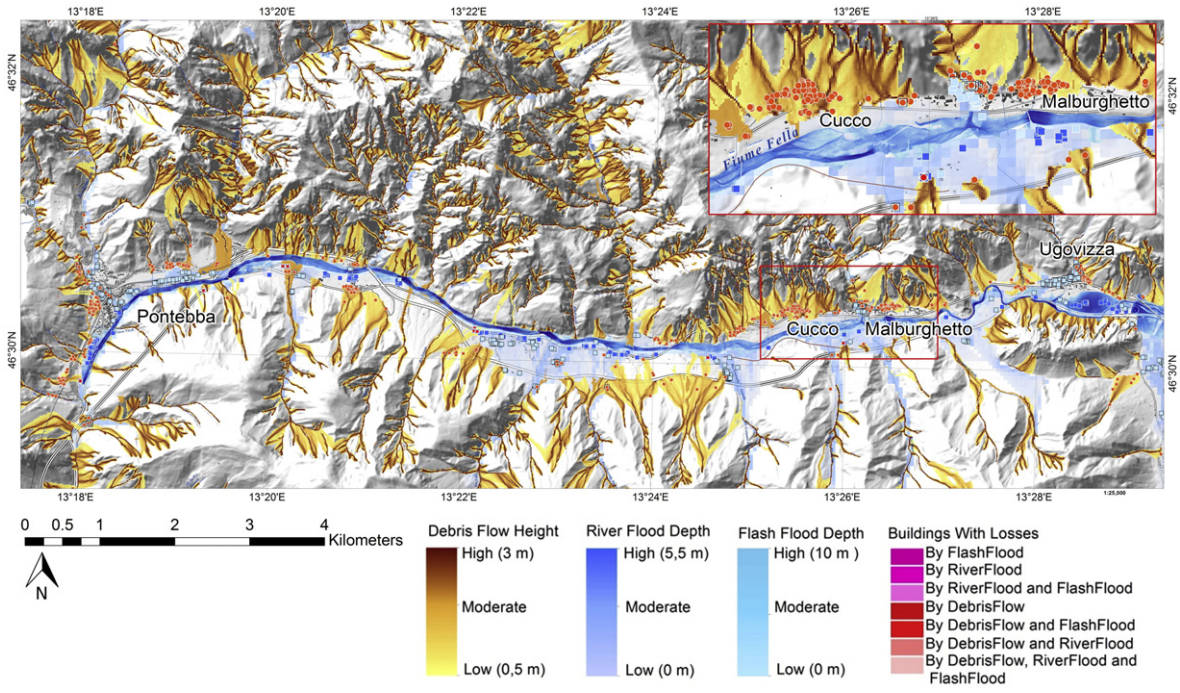

Fig. 12. Exposure map of buildings to debris flow, flash flood and river flood for the major hazard scenario. Inset map shows details of the most affected area in 2003.

population vulnerabilities for people in single storey buildings, with the same level of intensity, as compared to multi-storey buildings. We did not differentiate between age classes or other characteristics, as this information was not available.

As damage data in the aftermath of the 2003 event were insufficient to generate vulnerability curves for all building and hazard types, we developed a number of curves through expert opinion and logical reasoning. We started with the curves for which we had data and extended them to similar types of structures, with different numbers of floors. Most of the population vulnerability curves were constructed by ourselves due to lack of suitable information from literature. The resulting average curves are shown in Fig. 11. The vulnerability curves can also be represented by equations, although this might require the subdivision of a curve in different equations for different ranges of intensity. In order to calculate losses, it was more convenient to represent the data in vulnerability tables where the minimum, average and maximum vulnerability is given per intensity class.

4.7. Multi-hazard risk assessment

Losses for the individual hazard types and hazard scenarios were calculated by multiplying the spatial probability of the element-at-risk being impacted by the hazard, the physical vulnerability and the quantification of the exposed elements-at-risk (Fig. 3 and Eq. 1). We used a total of 36 different hazard maps, representing three hazard types (debris flows, river flooding and flash flooding), each having four hazard-scenarios (major, moderate, minor and frequent events), and calculating the minimum, average and maximum intensity values for each scenario. An example of the multi-hazard exposure map (major scenario) for the most affected part of the study in 2003 between Pontebba and Ugovizza is shown in Fig. 12. This figure shows that most exposed buildings are located at the base of the slopes, or on alluvial fans of small tributaries, where debris flows and flash flood are most likely to occur. It is also clear that more buildings are located in the influence areas of debris flows and flash floods than in the zones close to the river.

The resulting minimum and maximum losses for the hazard types and the four hazard-scenarios are presented in Table 6. For debris flows and flash floods we calculated for each element-at-risk the maximum loss, since many elements are exposed to both processes. Generally, the losses for debris flows and flash floods are one to six times higher than for river flood events, with the exception of the frequent hazard-scenario, where river flood losses are higher than debris flow and flash flood losses. For debris flows, the monetary loss associated with the major scenario is more than 500,000 times higher than that for the frequent event, with a loss ranging from 15 to 22 million euros in

Table 6
Economic losses (in thousands of euro) and casualties for hazard types under different hazard scenarios.

Hazard types	Hazard scenario	Exposure				Losses			
		Buildings		Population		Economic losses to buildings (*1000 €)		Population losses (persons)	
		Min.	Max.	Min.	Max.	Min.	Max.	Min.	Max.
River flood	Major	122	214	103	119	4680	6730	4	10
	Moderate	58	129	45	52	3380	4870	1	2
	Minor	61	94	33	38	147	207	0	1
	Frequent	30	77	25	29	14	20	0	0
Debris flows & flash flood	Major	453	793	272	715	15,800	22,200	77	99
	Moderate	136	305	127	445	2940	4080	15	74
	Minor	67	104	49	85	931	1310	3	10
	Frequent	7	7	6	6	31	40	0	0

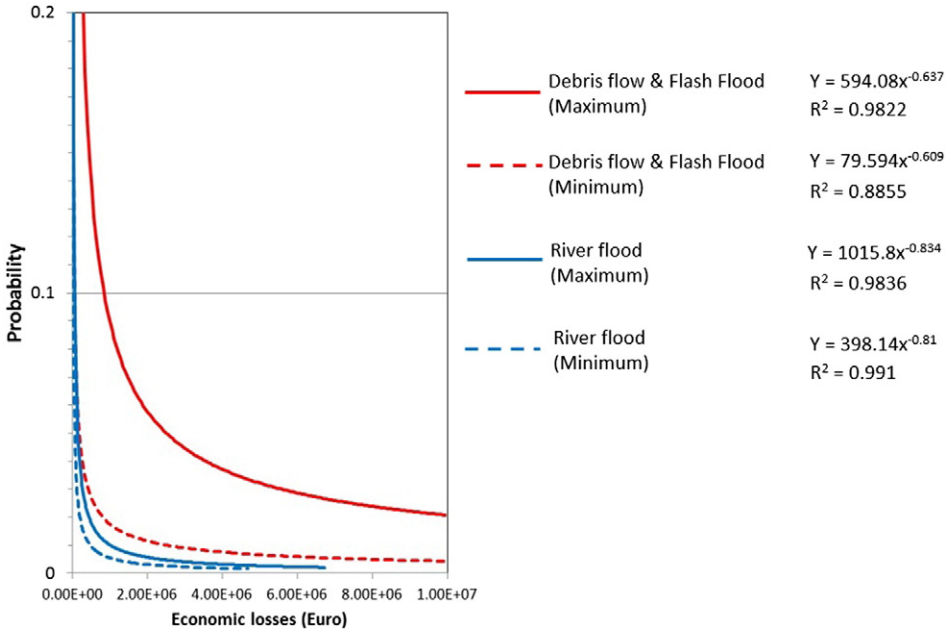

Fig. 13. Risk curves by plotting economic loss against annual probability.

direct economic damage. The losses in terms of casualties seem to be very high, especially for debris flows and flash floods, with a maximum of 99 casualties for a major hazard-scenario.

The risk was represented by risk curves, plotting losses (Table 6) against annual probability of the hazard scenarios (Table 3) (Van Westen et al., 2002). Fig. 13 displays the risk curves for economic losses, showing the large variation in risk for debris flow and flash flood as compared to river flood. The average annual losses, which are the areas under the risk curves in Fig. 13 are presented in Table 7. The results show that the expected losses for debris flows and flash flood are much higher than for river flood, because the hazard areas are much larger and many of the settlements are located in the debris flow and flash flood hazard areas. The debris flow and flash flood losses show a large variation between the minimum and maximum expected losses. This illustrates the large uncertainties in the various hazard components that are used in the risk equation: temporal probability of the hazard scenario, hazard intensity and spatial probability that modelled debris flow cells will be actually affected in a real event.

5. Validation

It is generally difficult to validate the results of a risk analysis. The only option is to compare the calculated losses with those of similar events that have occurred in the past. We cannot compare or validate it with examples from other areas, as this would require a similar exercise including hazard modelling, elements-at-risk assessment and vulnerability assessment. We were able to collect damage information for the large disaster event in 2003, which was considered as a major hazard scenario (Table 3). The direct comparison of the damage from this historical event with the present risk situation may also present problems, because in between the two dates there may have been large changes in the number of buildings and people. For example the buildings that were destroyed in the historical event of 2003, might not have been rebuild in the same location, and in other areas new building might have been constructed.

The modelled monetary losses related to buildings and casualties were compared with the losses from the 2003 event reported by the Italian Civil Protection. The reported economic damage for the communes that were included in this study (Malburghetto, Tarvisio, Pontebba and Dogna) related to damage to private and commercial buildings was 59.1 million euro. These were much larger than the modelled losses resulting from our analysis, which are 22.2 Million Euro for debris flows and flash floods and 6.73 million for river flood. However, one should bear in mind that the modelled economic losses were only related to private buildings, as we did not have enough data to model losses to commercial and industrial facilities. Furthermore, the modelling was carried out using the present building stock, excluding those destroyed by the 2003 event. Also several mitigation works have been constructed since 2003. The available reported casualty statistics for the 2003 event indicated that two people were killed during the event. The number of casualties that we modelled for this event is larger (Table 7). This is due to a number of factors, related to the use of single casualty vulnerability functions, instead of separate ones for injuries. Another important reason is warnings and evacuations of the population are not considered in our study. In 2003, local civil protection and voluntary fire brigades were alerted 1 day before the extreme event, and approximately 600 people were evacuated in Malburghetto Municipality alone (FloodSite Project, 2007; Scolobig et al., 2008).

6. Discussion and conclusions

The results of this research show that the average annual economic risk for debris flows and flash floods (1.369 million euro if maximum values are used) can be more than 10 times higher than the risk of

Table 7
Average annual economic and population loss due to river flood and to the combination of debris flow and flash flood.

Hazard type	Economic losses (million euro)			Casualties (persons killed)		
	Minimum	Average	Maximum	Minimum	Average	Maximum
River flood	0.055	0.085	0.108	0.008	0.009	0.011
Debris flow & flash flood	0.192	0.835	1.369	1.074	3.891	7.592

river flood (0.108 million euros). This is even more pronounced for population risk (Table 7). The uncertainty of the estimated losses is generally equally high for both hazard types. The annual economic risk for debris flows and flash floods for instance, varies between 0.19 and 1.37 million euros, and the annual population risk between 1 and 7.5 persons.

The method we selected for expressing uncertainties in the losses using minimum, average and maximum values is a practical method that can be understood by stake-holders, as was also demonstrated by Komendantova et al. (2014) who compared the stakeholders' perceptions of different multi-risk models. The results of this work were presented to the stakeholders in the study area, consisting of mayors, planners and representatives of the local and regional Civil Protection Agency during a workshop in November 2014, during which they indicated that the result were very useful for disaster risk reduction planning.

As is illustrated in Fig. 1, the maximum and minimum ranges of the risk curves are determined by a number of factors: the probability ranges of the identified hazard scenarios (which come directly from the return periods used) along the Y-axis and the multiplication of the vulnerability and the quantification of the exposed assets along the X-axis. The definition of the hazard scenarios, as indicated in Table 3, forms the basis for the subdivision of hazard events and their return periods. As can be seen from the comparison of the expert-based range of return periods with the (limited) representative events the return period range is taken in such a way that the maximum return period of one scenario (e.g. minor: 10–25 years) is the minimum of the higher class (e.g. moderate: 25–100 years).

The relatively large range of uncertainty in the calculated losses is related to a number of factors. One of the main sources of uncertainty is related to the definition of the hazard scenarios and the associated return periods (Table 3). As historical debris flow and flood event dates are difficult to reconstruct, and the number of available dates was rather limited, the relation between these historical events and the triggering rainfall amount has a considerably range of uncertainty, as represented by the values given in Table 3. Another important component leading to uncertainty is the hazard intensity modelling. Debris flow intensity values were obtained using an empirical regional-scale debris flow run-out model in Flow-R, in which the run-out probability was used in combination with a transfer function to convert the results into debris flow height intensity, based on a selected number of back analysed debris flows with Flo-2D. The correlation between the Flow-R probability classes and the Flo-2D flow depth of $R^2 = 0.84$ can be considered strong, but there were still uncertainties due to the classification process of the original Flow-R probabilities into 10 quantile classes. From a geomorphological point of view the main challenge in the risk modelling is related to the modelling of various geomorphological processes (flash floods, debris flows and river floods) that are triggering during the same extreme rainfall event. Due to a lack of models that analyse these processes and their interactions simultaneously, we used models that analysed them separately. We decided to combine the losses for debris flows and flash floods in this study, as these processes often affect the same locations, and are triggered by the same rainfall event. During such a triggering event they might even alternate in the same subcatchment. Therefore we used only the maximum loss either from debris flows or from flash flooding in the final analysis. We decided to keep the loss estimation for river flood separately in order to compare it with the debris flow and flash flood losses. We are currently developing such a combined hydro-meteorological hazard modelling tool, based on the OpenLISEM model for rainfall-runoff modelling, by incorporating a soil hydrology component, linked with a slope stability analysis, so that interactions among landslides, debris flows and flash floods can be modelled for the same rainfall events.

The elements-at-risk database is another source of uncertainty, in particular related to the estimation of building values and the number of people per building. However, the results obtained for the non-tourist season scenario seem to compare reasonably well with the official statistical data. The quantification of the exposed elements-at-risk depends on two factors: the number of exposed elements-at-risk and the quantification method. The number of exposed elements-at-risk depends again much on the hazard modelling outputs, and the variation of the input parameters for modelling. The quantification of the elements-at-risk depends on the available information on aspects like building values and population, and the detail of the mapped building stock, in terms of occupancy types and floor spaces.

Another source of uncertainty in the risk modelling are the vulnerability curves, which were derived using a compilation of existing curves from literature, a limited correlation of historical damage and intensity data, and mostly using expert opinion. Unfortunately, there are still no libraries of vulnerability curves available for different building types and hazard intensities types, although there are several attempts under way to develop these (Papathoma-Köhle et al., 2012). The range of vulnerability depends on two factors: the range of intensities of the hazard phenomena and the definition of the curves. The intensities of the hazard phenomena determine the range on the X-axis in the vulnerability curves (Fig. 11). The range of intensity results from the hazard modelling, which again depends on the input parameter ranges used.

Further research is needed to reduce the uncertainty in multi-hazard risk assessment for mountainous environments, though improved models for hazard interaction analysis and the generation of libraries of building and population related vulnerability curves for debris flows and flash flood in different mountainous environments. The location of people during an event and the effect of warnings and evacuations should also be considered in order to decrease the overestimation of population risk.

Acknowledgements

This research was carried in the framework of the EU FP7 Marie Curie Project CHANGES (www.changes-itn.eu), under Grant Agreement No. 263953, and the EU FP7 Copernicus project INCREO (http://www.increo-fp7.eu), under Grant Agreement No. 312461, funded by the European Community's Seventh Framework Programme, FP7/2007–2013. Within these projects a Spatial Decision Support System, RiskChanges, was generated to carry out a multi-hazard risk assessment as described in this research. The system is online, and can be accessed through the following URL: http://changes.itc.utwente.nl/RiskChanges/.

The authors would like to thank Simone Frigerio and Alessandro Pasuto (CNR-IRPI, Padua), Claudio Carlati (Civil Protection of Regione Autonoma Friuli Venezia Giulia), Geological Survey of the FVG Region, and Dr. Chiara Calligaris for their support in data collection. Simone Sterlacchini (CNR-IDPA, Milano, Italy) and Paola Reichenbach (SNR-IRPI, Perugia) are thanked for their support in debris flow susceptibility assessment. We would like to thank Ziga Malek (Free University Amsterdam) for his support in land use change models. Zar-Chi Aye (University of Lausanne, Switzerland) is thanked for her support in the development of the SDSS, and Teresa Sprague (University of Dortmund), Kathrin Prenger-Berninkhoff (University of Aachen), Juliette Cortes and Marie Charriere (Technical University Delft) are thanked for their help with stakeholder interaction. We also would like to thank Nelson Caine, Francisco Gutierrez and Tagashi Oguchi for their constructive reviews.

References

Agenzia delle Entrate, 2013. Building values for Fella area. (URL: http://www.tuttitalia.it/friuli-venezia-giulia/91-pontebba/).

Akbas, S., Blahut, J., Sterlacchini, S., 2009. Critical assessment of existing physical vulnerability estimation approaches for debris flows. In: Walter, M., Joswig, M. (Eds.), Landslide Processes: From Geomorphological Mapping to Dynamic Modelling. CERG Editions, Strasbourg, pp. 229–233.

Bell, R., Glade, T., 2004. Multi-hazard analysis in natural risk assessments. International Conference on Computer Simulation in Risk Analysis and Hazard Mitigation, Brebbia, C.A., Rhodes, Greece, pp. 197–206.
Blahut, J., Horton, P., Sterlacchini, S., Jaboyedoff, M., 2010. Debris flow hazard modelling on medium scale: Valtellina di Tirano, Italy. Nat. Hazards Earth Syst. Sci. 10, 2379–2390.
Bonham-Carter, G., Agterberg, F., Wright, D., 1988. Integration of geological datasets for gold exploration in Nova Scotia. Digital Geologic and Geographic Information Systems, pp. 15–23.
Bovolo, C.I., Abele, S.J., Bathurst, J.C., Caballero, D., Ciglan, M., Eftichidi, G., Simo, B., 2009. A distributed framework for multi-risk assessment of natural hazards used to model the effects of forest fire on hydrology and sediment yield. Comput. Geosci. 35, 924–945.
Buonomo, E., Jones, R., Huntingford, C., Hannaford, J., 2007. On the robustness of changes in extreme precipitation over Europe from two high-resolution climate change simulations. Q. J. R. Meteorol. Soc. 133 (622), 65–81.
Calligaris, C., Boniello, M.A., Zini, L., 2008. Debris flow modelling in Julian Alps using FLO-2D. In: De Wrachien, D., Brebbia, C.A., Lenzi, M.A. (Eds.), Monitoring, Simulation, Prevention and Remediation of Dense and Debris Flows II. WIT Press, Southampton, UK, pp. 81–88.
Cardona, O.D., Schroder, O., Gustavo, M., Reinoso, E., Yamín, L., Barbat, A., Horia, A., 2010. Comprehensive approach for probabilistic risk assessment (CAPRA): international initiative for disaster risk management effectiveness. International Symposium on Reliability Engineering and Risk Management, Shanghai, 2010, pp. 1–10.
Carpignano, A., Golia, E., Di Mauro, C., Bouchon, S., Nordvik, J.-P., 2009. A methodological approach for the definition of multi-risk maps at regional level: first application. Journal of Risk Research 12 (3–4), 513–534.
Castellanos Abella, E.A., de Jong, S.M., van Westen, C.J., van Asch, T.W.J., 2008. Multi-scale Landslide Risk Assessment in Cuba (Ph.D. Thesis) Faculty of Geo-information Science and Earth Observation, Enschede, The Netherlands.
CNR-IRPI, 2014. AVI Project. (URL http://avi.gndci.cnr.it/en/archivi/frane_en.htm).
Dahal, R.K., Hasegawa, S., Nonomura, A., Yamanaka, M., Masuda, T., Nishino, K., 2008. GIS-based weights-of-evidence modelling of rainfall-induced landslides in small catchments for landslide susceptibility mapping. Environ. Geol. 54, 311–324.
Del Monaco, G., Margottini, C., Serafini, S., 1999. Multi-hazard risk assessment and zoning: an integrated approach for incorporating natural disaster reduction into sustainable development. Technical Report, TIGRA project (The Integrated Geological Risk Assessment), Grant No. Env4-CT96-0262. European Commission DG XII, Environment and Climate Program, Brussels.
Del Monaco, G., Margottini, C., Spizzichino, D., 2007. ARMONIA methodology for multi-risk assessment and the harmonisation of different natural risk map. Technical Report D3.1.1, ARMONIA Project (Applied Multi-Risk Mapping of Natural Hazards for Impact Assessment), Grant No. 511208. Rome, 31 January 2007.
Dilley, M., Chen, R.S., Deichmann, U., Lerner-Lam, A.L., Arnold, M., 2005. Natural Disaster Hotspots: A Global Risk Analysis. The World Bank Hazard Management Unit, Washington, D.C.
Douglas, J., 2007. Physical vulnerability modelling for natural hazards risk assessment. Nat. Hazards Earth Syst. Sci. 7, 283–288.
Dutta, D., Herath, S., Musiake, K., 2003. A mathematical model for flood loss estimation. J. Hydrol. 277 (1–2), 24–49.
EEA, 2014. CORINE Land Cover Programme of the European Environment Agency. (URL http://www.eea.europa.eu/publications/COR0-landcover).
Eidsvig, U., Papathoma-Kohle, M., Du, J., Glade, T., Vangelsten, B., 2014. Quantification of model uncertainty in debris flow vulnerability assessment. Eng. Geol. 181, 15–26.
Finlay, P.J., 1996. The Risk Assessment of Slopes (Ph.D. Thesis) University of New South Wales, Australia.
FloodSite Project, 2007. Risk contribution and social vulnerability in an Italian Alpine Region. (www.floodsite.net).
Fuchs, S., Heiss, K., Huebl, J., 2007. Towards an empirical vulnerability function for use in debris flow risk assessment. Nat. Hazards Earth Syst. Sci. 7, 495–506.
Garcia-Aristizabal, A., Gasparini, P., Uhinga, G., 2015. Multi-risk assessment as a tool for decision-making. In: Pauleit, S., Coly, A., Fohlmeister, S., Gasparini, P., Jørgensen, G., Kabisch, S., Kombe, W.J., Lindley, S., Simonis, I., Yeshitela, K. (Eds.), Urban Vulnerability and Climate Change in Africa. Future City 4, pp. 229–258.
Garcia-Aristizabal, A., Marzocchi, W., 2013. Software for multi-hazard assessment. Deliverable 3.5 of the EU Matrix project: new methodologies for multi-hazard and multi-risk assessment methods for Europe. (URL: http://matrix.gpi.kit.edu/downloads/MATRIX-D3.05.pdf).
Godfrey, A., Ciurean, R.L., van Westen, C.J., Kingma, N.C., Glade, T., 2015. Assessing vulnerability of buildings to hydro-meteorological hazards using an expert based approach – an application in Nehoiu Valley, Romania. Int. J. Disaster Risk Reduct. 13, 229–241.
Granger, K., Jones, T.G., Leiba, M., Scott, G., 1999. Community Risk in Cairns: A Multi-hazards Risk Assessment. Technical report, Australian Geological Survey Organisation (AGSO) (URL http://www.ga.gov.au/corporate_data/33548/33548.pdf).
Green, W.H., Ampt, G.A., 1911. The flow of air and water through soils. J. Agric. Sci. 4, 11–24.
Gruber, E.E., Mergili, M., 2013. Regional-scale analysis of high-mountain multi-hazard and risk indicators in the Pamir (Tajikistan) with GRASS GIS. Nat. Hazards Earth Syst. Sci. 13, 2779–2796.
Grunthal, G., Thieken, A.H., Schwarz, J., Radtke, K.S., Smolka, A., Merz, B., 2006. Comparative risk assessments for the city of Cologne - storms, floods, earthquakes. Nat. Hazards 38 (1), 21–44 (URL http://link.springer.com/article/10.1007/s11069-005-8598-0).
Heinimann, H.R., Hollenstein, K., Keinholz, H., Krummenacher, B., Mani, P., 1998. Methoden zur Analyse und Bewertung von Naturgefahren. Umwelt-Materialien Nr. 85. Bundesamt für Umwelt, Wald und Landschaft (BUWAL), Bern, Switzerland.
Hollenstein, K., 2005. Reconsidering the risk assessment concept: standardizing the impact description as a building block for vulnerability assessment. Nat. Hazards Earth Syst. Sci. 5, 301–307.
Horton, P., Jaboyedoff, M., Bardou, E., 2008. Debris flow susceptibility mapping at a regional scale. In: Locat, J., Perret, D., Turmel, D., Demers, D., Leroueil, S. (Eds.), 4th Canadian Conference on Geohazards: From Causes to Management. Presse de l'Universite Laval, pp. 399–406.
Horton, P., Jaboyedoff, M., Rudaz, B., Zimmermann, M., 2013. Flow-R, a model for susceptibility mapping of debris flows and other gravitational hazards at a regional scale. Nat. Hazards Earth Syst. Sci. 13, 869–885.
Hufschmidt, G., Glade, T., 2010. Vulnerability analysis in geomorphic risk assessment. In: Alcántara-Ayala, I., Goudie, A.S. (Eds.), Geomorphological Hazards and Disaster Prevention. Cambridge University Press, Cambridge, pp. 233–243.
Hussin, H.Y., Chen, L., Ciurean, R., Van Westen, C.J., Reichenbach, P., 2014. Analysing changes in landslide risk using multi temporal landslide susceptibility and run-out modeling on a regional scale. International Conference on Analysis and Management of Changing Risks for Natural Hazards (URL http://www.changes-itn.eu/Portals/0/Content/2014/Final%20conference/abstracts/DO3_Abstract_Hussin_et_al.pdf).
Hussin, H.Y., Zumpano, V., Reichenbach, P., Sterlacchini, S., Micu, M., Bălteanu, D., Van Westen, C.J., 2016. Different landslide sampling strategies in a grid-based bi-variate statistical susceptibility model. Geomorphology 253, 508–523.
ISPRA, 2014. The IFFI Project: Inventory Of Landslide Phenomena in Italy. (URL http://www.isprambiente.gov.it/en/projects/iffi-project).
ISTAT, 2014. Italian National Institute of Statistics- ISTAT. (URL http://www.istat.it/).
ITC, 2015. The Integrated Land and Water Information System. (URL http://52north.org/communities/ilwis/ilwis-open).
Jetten, V., 2013. OpenLISEM-A Spatial Model for Runoff, Floods and Erosion. (URL http://blogs.itc.nl/lisem).
Jonkman, S.N., Bočkarjova, M., Kok, M., Bernardini, P., 2008. Integrated hydrodynamic and economic modelling of flood damage in the Netherlands. Ecol. Econ. 66 (1), 77–90.
JRC, 2014. MOLAND - Monitoring Land Use/Cover Dynamics.
Kappes, M., Keiler, M., Glade, T., 2010. From single to multi-hazard risk analyses: a concept addressing emerging challenges. In: Malet, J.P., Glade, T., Casagli, N. (Eds.), Mountain Risks: Bringing Science to Society. Proceedings of the International Conference, Florence. CERG Editions, Strasbourg, pp. 351–356.
Kappes, M.S., Malet, J.P., Remaitre, A., Horton, P., Jaboyedoff, M., Bell, R., 2011. Assessment of debris-flow susceptibility at medium-scale in the Barcelonnette Basin, France. Nat. Hazards Earth Syst. Sci. 11, 627–641.
Kappes, M.S., Keiler, M., Von Elverfeldt, K., Glade, T., 2012. Challenges of analyzing multi-hazard risk: a review. Nat. Hazards 64 (2), 1925–1958.
Karssenberg, D., Schmitz, O., Salamon, P., De Jong, K., Bierkens, M.F., 2010. A software framework for construction of process-based stochastic spatio-temporal models and data assimilation. Environ. Model Softw. 25, 489–502.
Kaynia, A.M., Papathoma-Köhle, M., Neuhäuser, B., Ratzinger, K., Wenzel, H., Medina Cetina, Z., 2008. Probabilistic assessment of vulnerability to landslide: application to the village of Lichtenstein, Baden-Württemberg, Germany. Eng. Geol. 101, 33–48.
Komendantova, N., Mrzyglocki, R., Mignan, A., Khazai, B., Wenzel, F., Patt, A., Fleming, K., 2014. Multi-hazard and multi-risk decision-support tools as a part of participatory risk governance: Feedback from civil protection stakeholders. Int. J. Disaster Risk Reduct. 8, 50–67.
Lari, S., Frattini, P., Crosta, G.B., 2009. Integration of natural and technological risks in Lombardy, Italy. Nat. Hazards Earth Syst. Sci. 9, 2085–2106.
Li, Z., Nadim, F., Huang, H., Uzielli, M., Lacasse, S., 2010. Quantitative vulnerability estimation for scenario-based landslide hazards. Landslides 7 (2), 125–134.
Liu, Z., Nadim, F., Vangelsten, B.V., Eidsvig, U., Kalsnes, B., 2014. Quantitative multi-risk modelling and management using Bayesian networks. In: Sassa, K., Canuti, P., Yin, Y. (Eds.), Landslide Science for a Safer Geoenvironment. Springer (URL http://link.springer.com/chapter/10.1007/978-3-319-05050-8_119).
Malek, Ž., Scolobig, A., Schröter, D., 2014. Understanding land cover changes in the Italian Alps and Romanian Carpathians combining remote sensing and stakeholder interviews. Land 3 (1), 52–73.
Manca, P., Kranitz, F., Oberti, S., Piano, C., 2007. Analisi del dissesto da frana in Friuli Venezia Giulia. In: Trigila, A. (Ed.), Rapporto sulle frane in Italia. Il Progetto IFFI - Metodologia, risultati e rapporti regionali. Rapporti 78/2007. APAT.
Marchi, L., Cavalli, M., Sangati, M., Borga, M., 2009. Hydrometeorological controls and erosive response of an extreme alpine debris flow. Hydrol. Process. 23, 2714–2727.
Martha, T.R., van Westen, C.J., Kerle, N., Jetten, V., Vinod, K.K., 2013. Landslide hazard and risk assessment using semi-automatically created landslide inventories. Geomorphology 184, 139–150.
Marzocchi, W., Mastellone, M.L., Di Ruocco, A., Novelli, P., Romeo, E., Gasparini, P., 2009. Principles of multi-risk assessment: interactions amongst natural and man-induced risks. Project Report (FP6 NARAS Project), European Commission, Directorate-General Research – Environment, Contract No. 511264. Office for Official Publications of the European Communities, Luxembourg.
Marzocchi, W., Garcia-Aristizabal, A., Gasparini, P., Mastellone, M.L., Di Ruocco, A., 2012. Basic principles of multi-risk assessment: a case study in Italy. Nat. Hazards 62, 551–573.
Merz, B., Thieken, A.H., 2009. Flood risk curves and uncertainty bounds. Nat. Hazards 51 (3), 437–458.
Mignan, A., Wiemer, S., Giardini, D., 2014. The quantification of low probability-high consequences events: part I. A generic multi-risk approach. Nat. Hazards 73, 1999–2022.
Ming, X.D., Xu, W., Li, Y., Du, J., Liu, B., Shi, P., 2015. Quantitative multi-hazard risk assessment with vulnerability surface and hazard joint return period. Stoch. Env. Res. Risk A. 29 (1), 35–44.
Nadim, F., Liu, Z., Garcia-Aristizabal, A., Woo, G., Aspinall, W., Fleming, K., Vangelsten, B.V., van Gelder, P., 2013. Framework for multi-risk assessment. Technical report D5.2,

MATRIX Project (New Methodologies for Multi-hazard and Multi-risk Assessment Methods for Europe), Grant No. 265138 (URL http://matrix.gpi.kit.edu/Deliverables.php).
Neuhauser, B., Terhorst, B., 2007. Landslide susceptibility assessment using weights-of-evidence applied to a study area at the Jurassic escarpment (SW-Germany). Geomorphology 86 (1–2), 12–24.
Papathoma-Köhle, M., Kappes, M., Keiler, M., Glade, T., 2011. Physical vulnerability assessment for Alpine hazards-state of the art and future needs. Nat. Hazards 58 (2), 645–680.
Papathoma-Köhle, M., Keiler, M., Totschnig, R., Glade, T., 2012. Improvement of vulnerability curves using data from extreme events: debris flow event in South Tyrol. Nat. Hazards 64 (3), 2083–2105.
Penning-Rowsell, E., Johnson, C., Tunstall, S., Tapsell, S., Morris, J., Chatterton, J., Green, C., 2005. The Benefits of Flood and Coastal Risk Management: A Handbook of Assessment Techniques. Flood Hazard Research Centre, Middlesex University.
Quan Luna, B., Blahut, J., Van Westen, C.J., Sterlacchini, S., Van Asch, T.W.J., Akbas, S.O., 2011. The application of numerical debris flow modelling for the generation of physical vulnerability curves. Nat. Hazards Earth Syst. Sci. 11, 2047–2060.
Ragozin, A.L., Tikhvinsky, I.O., 2000. Landslide hazard, vulnerability and risk assessment. In: Bromhead, E., Dixon, N., Ibsen, M.L. (Eds.), Proceedings of the 8th International Symposium on Landslides, Cardiff, pp. 1257–1262.
Reese, S., Ramsey, D., 2010. RiskScape: Flood fragility methodology. Wellington, New Zealand, National Institute of Water & Atmospheric Research Ltd (NIWA).
Rickenmann, D., Zimmermann, M., 1993. The 1987 debris flows in Switzerland: documentation and analysis. Geomorphology 8 (2), 175–189.
Sangati, M., Borga, M., 2009. Influence of rainfall spatial resolution on flash flood modelling. Nat. Hazards Earth Syst. Sci. 9, 575–584.
Sawatzky, D.L., Raines, G.L., Bonham-Carter, G.F., Looney, C.G., 2009. Spatial Data Modeller (SDM): ArcMAP 9.3 geoprocessing tools for spatial data modelling using weights of evidence, logistic regression, fuzzy logic and neural networks. (URL http://arcscripts.esri.com/details.asp?dbid=15341).
Schmidt, J., Matcham, I., Reese, S., King, A., Bell, R., Henderson, R., Smart, G., Cousins, J., Smith, W., Heron, D., 2011. Quantitative multi-risk analysis for natural hazards: a framework for multi-risk modelling. Nat. Hazards 58 (3), 1169–1192.
Schmidt-Tomé, P., Kallio, H., Jarva, J., Tarvainen, T., Greiving, S., Fleischhauer, M., Peltonen, L., Kumpulainen, S., Olfert, A., Schanze, J., Bärring, L., Persson, G., Relvão, A.M., Batista, M.J. (Eds.), 2006. The Spatial Effects and Management of Natural and Technological Hazards in Europe (ESPON) Project 1.3.1. Geological Survey of Finland (URL http://www.espon.lu).
Schneider, P.J., Schauer, B.A., 2006. HAZUS, its development and its future. Nat. Hazard. Rev. 7 (2), 40–44.
Scolobig, A., Castán Broto, V., Zabala, A., 2008. Integrating multiple perspectives in social multi-criteria evaluation of flood-mitigation alternatives: the case of Malborhetto-Valbruna. Environment and Planning C: Government and Policy 2008 (26), 1143–1161.
Totschnig, R., Fuchs, S., 2013. Mountain torrents: quantifying vulnerability and assessing uncertainties. Eng. Geol. 155, 31–44.
Tropeano, D., Turconi, L., Sanna, S., 2004. Debris flows triggered by the 29 August 2003 cloudburst in Val Canale, eastern Italian Alps. Proceedings of the 10th Internationales Symposion InterPraevent, Riva del Garda, Italy, pp. 121–132.
UNISDR, 2009. UNISDR terminology on disaster risk reduction. (URL: https://www.unisdr.org/we/inform/terminology).
USACE, 2000. U.S. army corps of engineers, Economic Guidance Memorandum (EGM) 01-03, generic depth- damage relationships. Economic Guidance Memorandum (EGM) 01-032000: Washington D.C.
Uzielli, M., Lacasse, S., 2007. Scenario-based probabilistic estimation of direct loss for geohazards. Georisk 1 (3), 142–154.
Van Westen, C.J., Kappes, M.S., Quan Luna, B., Frigerio, S., Glade, T., Malet, J.P., 2014. Medium-scale multi-hazard risk assessment of gravitational processes. In: van Asch, T., Corominas, J., Greiving, S., Malet, J.P., Sterlacchini, S. (Eds.), Mountain Risks: From Prediction to Management and Governance. Springer Netherlands, Dordrecht, pp. 201–231.
Van Westen, C.J., Montoya, A.L., Boerboom, L.G.J., Badilla Coto, E., 2002. Multi-hazard risk assessment using GIS in urban areas: a case study for the city of Turrialba, Costa Rica. Proceedings of the Regional Workshop on Best Practices in Disaster Mitigation: Lessons Learned From the Asian Urban Disaster Mitigation: Lessons Learned From the Asian Urban Disaster Mitigation Program and Other Initiatives, Bali, Indonesia, pp. 120–136.
Wilks, D., 2011. Statistical methods in the atmospheric sciences. International Geophysics Series 100. Elsevier.